New Proposal to Jefferson Lab PAC 19

Measurement of the Weak Pion-Nucleon Coupling Constant, h_π^1, in Parity-Violating Backward Pion Photoproduction near Threshold off the Proton

W. Bertozzi, D. W. Higinbotham, S. Gilad, S. Kowalski,
S. Sirca, R. Suleiman (spokesperson), Z. Zhou
Massachusetts Institute of Technology

P. A. Souder
Syracuse University

J. P. Chen, K. de Jager, J.-O. Hansen, J. LeRose, N. Liyanage,
R. Michaels, S. Nanda, A. Saha
Thomas Jefferson National Accelerator Facility

L. Kaufman, K. Kumar
University of Massachusetts

D. Margaziotis
California State University

C. C. Chang
University of Maryland

X. Jiang
Rutgers University

(A Hall A Collaboration Proposal)

December 14, 2000

Abstract

This proposal describes a measurement of the weak pion-nucleon coupling constant to a high level of accuracy using moderate beam time in a theoretically "clean" process. We propose to measure the parity-violating asymmetry in pion photoproduction off the proton, $\vec{\gamma}p \to n\pi^+$. This asymmetry is expected to be $\sim 2.3 \times 10^{-7}$, and can be measured to statistical uncertainty of $\sim 0.5 \times 10^{-7}$ at Jefferson Lab in Hall A. The systematic errors are expected to be smaller than the statistical errors. The asymmetry is related to the weak isovector pion-nucleon coupling, h_π^1, with no uncertainty due to nuclear structure. h_π^1 will be determined with uncertainty of 1.0×10^{-7}, 20% of its expected value, 4.6×10^{-7}. At present there are two experiments; photon circular polarization for ^{18}F ($|h_\pi^1| = 0.28^{+0.89}_{-0.28} \times 10^{-7}$) and the anapole moment of ^{133}Cs ($h_\pi^1 = 9.5 \pm 2.1\,[\text{exp.}] \pm 3.5\,[\text{theor.}] \times 10^{-7}$) that have been interpreted to give very different values of h_π^1. The disagreement in the extraction of h_π^1 from ^{18}F and ^{133}Cs systems could be a reflection of poor understanding of many-body physics. This experiment will be the first attempt to measure the weak pion-nucleon coupling constant in the single nucleon system. A reliable measurement of h_π^1 provides a crucial test of the meson-exchange picture of the weak nucleon-nucleon interaction. Such a test of the meson-exchange picture will shed light on low energy QCD.

1 Introduction

Parity invariance has played a critical role in the evolution of our understanding of the weak interaction. It was the experiment of Wu *et al.* [1] motivated by the suggestion of Lee and Yang [2] that led to reexamination of the symmetry properties of all interactions. In 1958, Feynman and Gell-Mann introduced the $V-A$ interaction for charged currents [3], which, when combined with Weinberg's introduction of the neutral current a decade later [4], essentially completed our picture of the weak force. Since that time careful experimental work has led to verification of nearly every aspect of the proposed weak interaction structure:

1. in the leptonic sector, $\mu^- \to e^-\nu_\mu\bar{\nu}_e, \tau^- \to e^-\nu_\tau\bar{\nu}_e$,
2. in the $\Delta S = 0, 1$ semi-leptonic sector, $n \to pe^-\bar{\nu}_e, \Lambda \to pe^-\bar{\nu}_e$,
3. in the $\Delta S = 1$ non-leptonic sector, $\Lambda \to p\pi^-, K^+ \to \pi^+\pi^0$.

However, there is one area missing from this itemization: The $\Delta S = 0$ non-leptonic nucleon-nucleon (NN) interactions, $NN \to NN$. Obviously there is nothing in the identity of the particles involved to reveal the difference between this weak interaction and the ordinary strong $NN \to NN$ process. In fact the weak NN component is masked by the much larger strong NN force but is detectable by the property of parity violation.

On the experimental side, the first search for parity violation in the NN interaction was carried out by Tanner [5] in 1957, but it was not until 1967 that convincing evidence

was presented for its existence by Lobashov *et al.* [6], who was able to find a $-6 \pm 1 \times 10^{-6}$ signal among the much larger parity-conserving strong background in radiative neutron capture from ^{181}Ta.

Purely hadronic weak interaction between nucleons can be mediated by the exchange of the $W^{\pm}$ and Z^0 bosons. At momentum transfers typical of the NN interaction, ~300 MeV/c, the appropriate degrees of freedom are mesons and nucleons. The range of the $W^{\pm}$ and Z^0 is $\sim 10^{-3}$ fm, much shorter than the distance between nucleons. The hard-core repulsion in the NN interaction keeps the nucleons much farther apart than the range of the weak gauge bosons. The long-range weak force between nucleons is mediated by the exchange of light mesons. As shown in Figure 1, a weak gauge boson, is emitted by a quark, travels a short distance, and changes into π, ρ, or ω, which then couples strongly to another nucleon. Therefore, at low energies ($E \leq 300$ MeV), the weak NN interaction is described in terms of an effective meson exchange model in which a meson is coupled to a nucleon via the weak interaction at one vertex and the strong interaction at the other. The order of magnitude of the weak meson-nucleon couplings (10^{-7}) can be estimated from a simple scaling argument relating the parity-violating and parity-conserving NN potentials $V_{NN}^{\rm pc}$ and $V_{NN}^{\rm pv}$, respectively:

$$\frac{V_{NN}^{\rm pv}}{V_{NN}^{\rm pc}} \sim G_F \, m_\pi^2 \sim 10^{-7} \ , \tag{1}$$

where $G_F = 1.01 \times 10^{-5} M_N^{-2}$ is the weak Fermi coupling constant.

The most comprehensive theoretical treatment to date to describe the weak NN interaction is given in a review by Desplanques, Donoghue, and Holstein (DDH) [7]. They used the non-relativistic quark model, weak SU(6) symmetry, current algebra, and strong SU(3) symmetry to relate known $\Delta S = 1$ hyperon decay amplitudes to the weak meson-nucleon couplings. Because of the hard-core repulsion in the NN interaction, it is customary to include only mesons of mass less than 800 MeV. Parity-violating π^0 and η exchanges would be also CP violating and are therefore suppressed by a factor of about 2×10^{-3}; as a result neutral pseudoscalar meson (π^0, η) are excluded from the model. Therefore, only $\pi^{\pm}, \rho$ and ω vertices need be considered and the form of the most general parity-violating effective Hamiltonian is:

$$\begin{aligned}
\mathcal{H}_{\rm wk} &= \frac{h_\pi^1}{\sqrt{2}} \bar{N} (\tau \times \pi)_3 N \\
&+ \bar{N} \left(h_\rho^0 \tau \cdot \rho^\mu + h_\rho^1 \rho_3^\mu + \frac{h_\rho^2}{2\sqrt{6}} (3\tau_3 \rho_3^\mu - \tau \cdot \rho^\mu) \right) \gamma_\mu \gamma_5 N \\
&+ \bar{N} (h_\omega^0 \omega^\mu + h_\omega^1 \tau_3 \omega^\mu) \gamma_\mu \gamma_5 N - h_\rho^{'1} \bar{N} (\tau \times \rho^\mu)_3 \frac{\sigma_{\mu\nu} k^\nu}{2M} \gamma_5 N \ .
\end{aligned} \tag{2}$$

There are in general seven unknown weak couplings. However, calculations indicate that $h_\rho^{'1}$ is quite small [8] and this term is generally omitted, leaving parity-violating observables to be described in terms of just six constants.

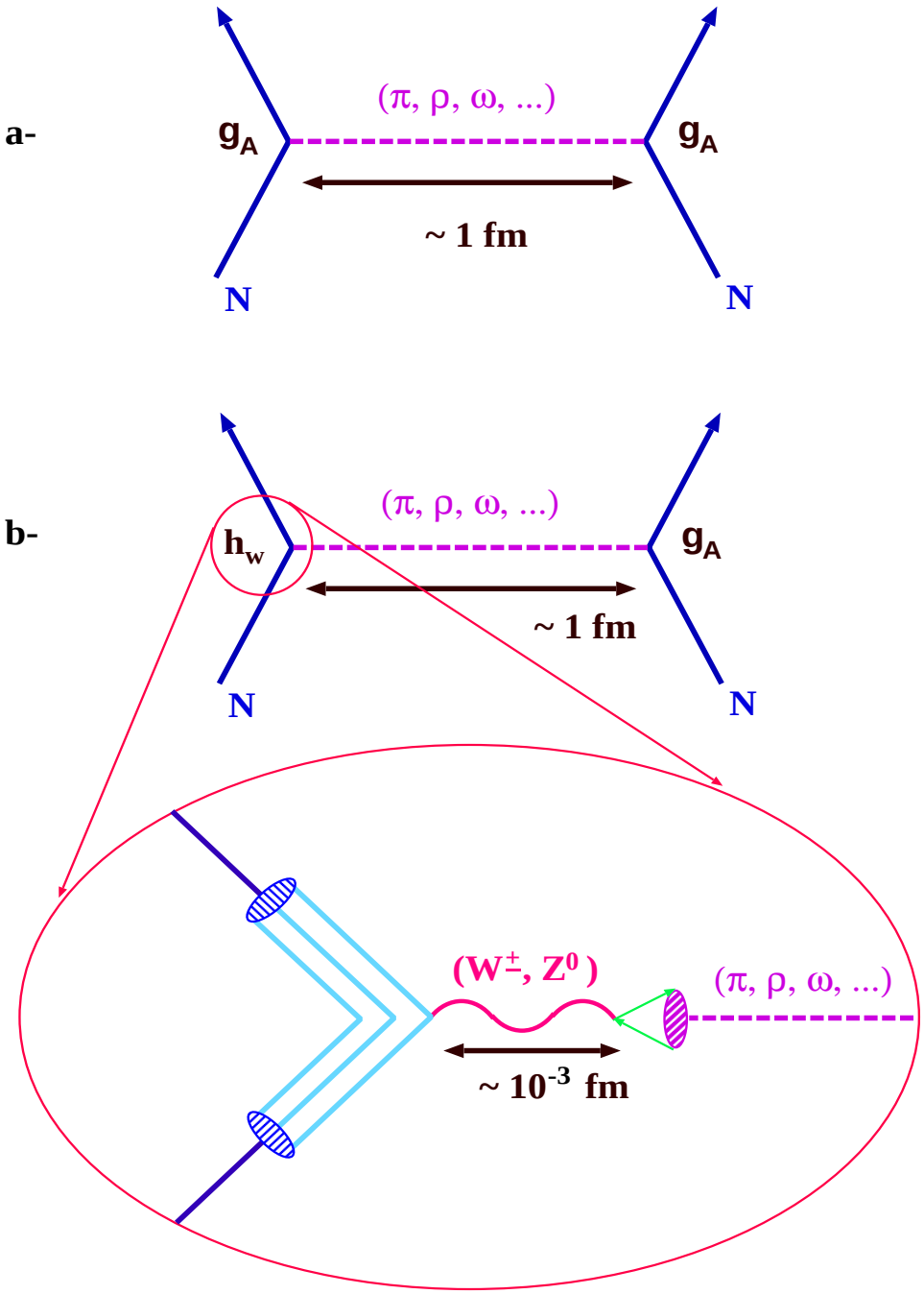

Figure 1: Meson-exchange model of the NN interaction at low energy. (a) Strong meson-exchange, $g_A \sim 1$. (b) Weak meson-exchange, $h_W \sim 10^{-7}$.

Because of uncertainties inherent in the quark model calculations, DDH reported their calculations in terms of broad "reasonable ranges" and "best guess values" of the weak NN interaction coupling constants h_π^1, h_ρ^0, h_ρ^1, h_ρ^2, h_ω^0, and h_ω^1 (labeled according to the meson exchange and the isospin exchanged ΔI at the vertex). The determination of these weak meson-nucleon coupling constants from experiment is an essential test of the weak meson-exchange model. The weak pion-exchange potential contributes only to isovector parity-violating processes, and as the pion is relatively light, its contribution is expected to dominate the weak isovector NN interaction at low energy.

1.1 Status of Our Knowledge of the Weak Meson-Nucleon Couplings

An extensive review of the theoretical and experimental work seeking to understand the phenomenon of parity violation within the nucleon-nucleon system is reviewed by Haeberli and Holstein in Reference [9] and by Desplaques in Reference [10]. A brief summary is given here.

1.1.1 Theoretical Calculations of the Weak Meson-Nucleon Couplings

DDH "best guess values" and "reasonable ranges" for the couplings are given in Table 1. Listed also in the same table, the theoretical predictions of Dubovik and Zenkin (DZ) [11] and of Feldman, Crawford, Dubach, and Holstein (FCDH) [12]. Adelberger and Haxton (AH) [13] extracted from the available data a "best fit" of the weak meson-nucleon couplings.

The estimate of h_π^1 from the quark model and weak SU(6) symmetry has been discussed above. Desplanques [14] revised the estimate of the "reasonable range" of h_π^1 to $0 \rightarrow 2.5 \times 10^{-7}$ and the "best value" to 2×10^{-7}. Recently, Henley, Hwang, and Kisslinger [15] used QCD sum rules to obtain h_π^1. They found that $h_\pi^1 = 3 \times 10^{-7}$, in good agreement with the prediction of DDH. Kaplan and Savage [16] estimated the size of h_π^1 using naive dimensional analysis. Their result of $h_\pi^1 \sim 5 \times 10^{-7}$ is similar to the dimensional estimate of DDH.

1.1.2 Previous Experiments

Measurement of P_γ from ^{18}F and its Interpretation:

The determination of the weak meson-nucleon exchange couplings from experimental measurements in nuclei are discussed in the review by Adelberger and Haxton [13]. There are substantial uncertainties in interpreting most experiments in nuclei because one can not make reliable calculations of the amplitudes of the weak meson-nucleon exchange potential operators. The circular polarization P_γ of the 1.081 MeV transition in ^{18}F is an exception to this unfortunate situation because the matrix elements needed to extract a value for h_π^1 from experiment can be measured experimentally. The circular polarization of

Coupling	Theoretical (10^{-7})				Experimental (AH) (10^{-7})	
	Range (DDH)	"Best Value" (DDH)	Value (DZ)	Value (FCDH)	Range	"Best Fit"
h_π^1	$0 \to 11.4$	4.6	1.3	2.7	$0 \to 11$	2.1
h_ρ^0	$-31 \to 11.4$	-11.4	-8.3	-3.8	$-32 \to 11$	-5.7
h_ρ^1	$-0.38 \to 0$	-0.19	0.39	-0.4	$-0.4 \to 0.4$	-0.2
h_ρ^2	$-11.0 \to -7.6$	-9.5	-6.7	-6.8	$-10 \to -6.3$	-6.8
h_ω^0	$-10.3 \to 5.7$	-1.9	-3.9	-4.9	$-12 \to 2.7$	-6.5
h_ω^1	$-1.9 \to -0.8$	-1.1	-2.2	-2.3	$-3.0 \to -1.1$	-2.3

Table 1: Theoretical estimates of the sizes of the weak meson-nucleon couplings.

a $\Delta I = 1$ parity forbidden gamma transition in ^{18}F has been measured in five different and internally consistent experiments [17]. These measurements gave $|h_\pi^1| = 0.28^{+0.89}_{-0.28} \times 10^{-7}$. This value is a fraction of DDH best guess and is an order of magnitude smaller than the reasonable range.

Measurement of the Anapole Moments of ^{133}Cs and ^{205}Tl and its Interpretation:

The non-zero measurement of the anapole moment of ^{133}Cs [18] has been analyzed by Flambaum and Murray [19] to extract a value for h_π^1. Their result, $h_\pi^1 = 9.5 \pm 2.1\,[\text{exp.}] \pm 3.5\,[\text{theor.}] \times 10^{-7}$, is a factor of two larger than the DDH value and a factor of seven larger than the upper limit set by the ^{18}F experiments. However, their analysis is controversial for two reasons [20]. First, the ^{133}Cs anapole moment is almost as sensitive to h_ρ^0 as to h_π^1. Secondly, the result from ^{133}Cs is inconsistent with an earlier null measurement of the anapole moment of ^{205}Tl [21]. The situation is summarized in Figure 2. The present controversy concerning the interpretation of measured nuclear anapole moments highlights the need to determine the weak couplings from experiments in few-nucleon systems and the single nucleon system whose interpretation is free from uncertainties in nuclear structures.

Experiments in the *pp* System:

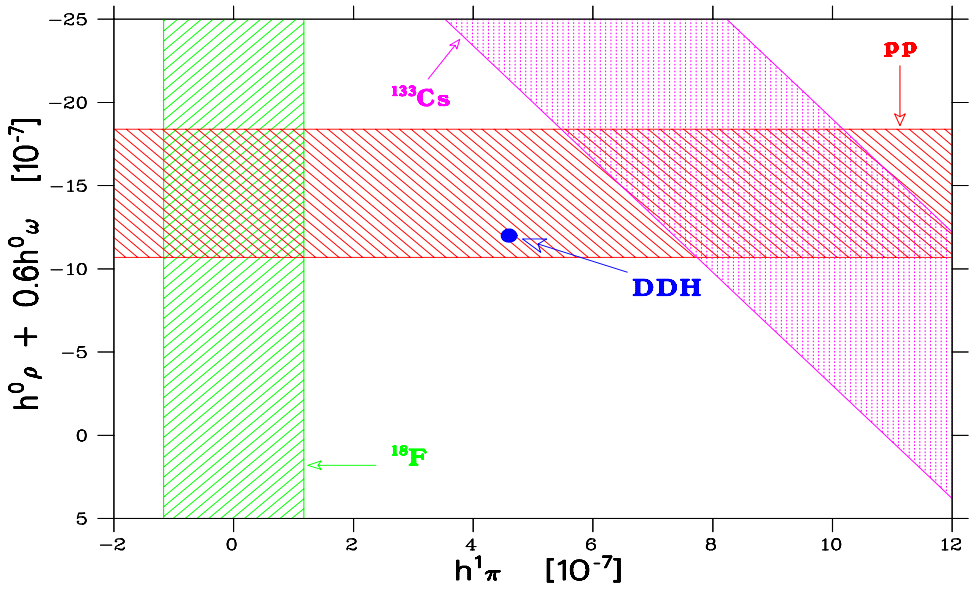

Figure 2: Plot of the constraints on the isoscaler and isovector weak meson-nucleon coupling constants.

An extensive program of high quality experiments has been carried out to measure the parity-violating longitudinal asymmetry A_z in the scattering of polarized protons off unpolarized protons at 13.6 MeV [$A_z = -0.93 \pm 0.20 \pm 0.05 \times 10^{-7}$] at the University of Bonn [22], and at 45 MeV [$A_z = -1.53 \pm 0.23 \times 10^{-7}$] at SIN in Switzerland (now PSI) [23]. Both results allow the determination of a combination of effective ρ and ω weak meson-nucleon coupling constants:

$$A_z = 0.153 \left(h^0_\rho + h^1_\rho + h^2_\rho/\sqrt{6}\right) + 0.113 \left(h^0_\omega + h^1_\omega\right) \ . \tag{3}$$

The TRIUMF 221.3 MeV experiment [24] is sensitive only to the ρ couplings:

$$A_z = -0.0296 \left(h^0_\rho + h^1_\rho + h^2_\rho/\sqrt{6}\right) \ , \tag{4}$$

(note that h^1_π does not enter due to CP violation).

There exist two further higher energy parity violation experiments. The first one is a $\vec{p}p$ parity violation measurement at 800 MeV with $A_z = 2.4 \pm 1.1 \times 10^{-7}$ at LANL [25]. Its interpretation in terms of the effective ρ and ω weak meson-nucleon coupling constants is more difficult due to the presence of a large inelastic contribution (pion production). The second one is a proton-nucleus parity violation measurement at 5.13 GeV on a water target with $A_z = 26.4 \pm 6.0 \pm 3.6 \times 10^{-7}$ at ANL with the ZGS [26]. This result is much larger than predictions based on meson-exchange calculations. New $\vec{p}p$ parity violation experiments are being planned at TRIUMF possibly at 450 MeV and with COSY at the

Forschungszentrum Jülich near 2 GeV as a storage ring experiment [27].

Experiments in the np System:

Measurements have been made in np capture of both the directional asymmetry A_γ and circular polarization of the emitted photons. Both experiments were statistically limited, and yielded null results. In the first case, Alberi *et al.* [28] reported a value of $A_\gamma = -0.15 \pm 0.47 \times 10^{-7}$, which gives $h_\pi^1 = -1.3 \pm 4.7 \times 10^{-6}$. In the second case, Knyaz'kov *et al.* [29] reported a value of $P_\gamma = 1.8 \pm 1.8 \times 10^{-7}$, which gives $h_\rho^0 + 2h_\rho^2/\sqrt{6} = 8.2 \pm 8.2 \times 10^{-6}$. The inverse reaction, deuteron photodisintegration by circularly polarized photons, has been measured by Earle *et al.* [30], who also report a null result. These experimental limits are less stringent that the reasonable ranges given in Table 1.

While the previous measurements could not reach the required precision, new experiments under way are expected to improve significantly. These include $\vec{n}p \to d\gamma$ at LANSCE [31]. This experiment will measure the directional asymmetry A_γ of the photons emitted in the capture process which is given by [13]:

$$A_\gamma = -0.107 \left(h_\pi^1 + 0.012 h_\rho^1 - 0.035 h_\omega^1 \right) \ . \tag{5}$$

In the experiment, neutrons from the spallation source are moderated by a liquid hydrogen moderator. The source is pulsed, thus allowing measurement of neutron energy through time-of-flight techniques. The cold neutrons are then polarized in the vertical direction by transmission through a polarized ^{3}He gas. The neutron spin direction can be subsequently reversed by a radio-frequency resonance spin flipper. The neutrons are then captured in a liquid para-hydrogen target. Photons emitted in the capture process are detected in an array of photon detectors surrounding the target. The parity-violating asymmetry causes an up-down asymmetry in the angular distribution of the photons for vertical neutron spin. When the neutron spin is reversed, the up-down photon asymmetry reverses. The parity-violating asymmetry in photon flux,

$$\frac{d\omega}{d\Omega} = \frac{1}{4\pi}(1 + A_\gamma \cos\theta_{s,\gamma}) \ , \tag{6}$$

is then a measure of h_π^1. LANSCE experiment will measure A_γ with a statistical error of 0.5×10^{-8} in two calendar years of data taking. The experimental uncertainty in the extracted value of h_π^1 will be 10% of the DDH estimate while the theoretical uncertainty is estimated to be 10% [32]. This experiment is expected to start commissioning and data taking in 2002. In 9 months of data it will achieve a statistical error of 10% [32].

Another planned experiment at Jefferson Lab [33] will measure the asymmetry in photodisintegration of the deuteron by circularly polarized photons, $\vec{\gamma}d \to np$. This experiment will measure a combination of the short distance (ρ and ω) weak coupling constants. The pion contribution to this asymmetry vanishes [34] and thus this experiment is not sensitive to h_π^1.

Experiments in the Single Nucleon System:

This experiment will be the first attempt to measure the weak meson-nucleon coupling constant in the single nucleon system. This measurement is free from nuclear structure uncertainties and is a clean measurement of h_π^1 [35] [36].

2 Pion Photoproduction

This experiment will measure h_π^1 by studying pion photoproduction, $\vec{\gamma}p \to n\pi^+$, with the detection of π^+. The weak interaction induced parity-violating asymmetries in low energy pion photoproduction were calculated to be of order 10^{-7} by Woloshyn [37] and by Li, Henley, and Hwang [38] in the frame work of meson exchange models. But it is Chen and Ji [35] who first identify the pion photoproduction off proton as an experimentally feasible and theoretically clean process to measure h_π^1. They found that the photon helicity asymmetry:

$$A_\gamma = \frac{d\sigma(\lambda_\gamma = +1) - d\sigma(\lambda_\gamma = -1)}{d\sigma(\lambda_\gamma = +1) + d\sigma(\lambda_\gamma = -1)} \tag{7}$$

at the first non-vanishing order (NLO) in heavy-baryon chiral perturbation theory (HBχPT) at threshold is:

$$A_\gamma(\vec{\gamma}p \to \pi^+ n)|_{\rm th} = \frac{\sqrt{2} f_\pi (\mu_p - \mu_n)}{g_A m_N} h_\pi^1 \sim h_\pi^1/2 \ , \tag{8}$$

where f_π is the pion decay constant ($f_\pi = 93$ MeV) and g_A is the neutron decay constant ($g_A = 1.257$). In this experiment, there is an extended threshold region in which the effective theory description remains effective and, at the same time, the cross section is appreciable. This region is between 180 and 230 MeV in laboratory photon energy. The higher-order corrections are expected to be $\mathcal{O}(E_\gamma/M_N) \sim 20\%$ and will be studied in the future [39]. Figure 3 shows the graphs contributing to the parity-conserving and parity-violating cross sections.

The total cross section for $\gamma p \to n\pi^+$ as a function of photon laboratory energy E_γ is shown in Figure 4. Also shown the $\gamma p \to p\pi^0$ total cross section. Data points are taken from Reference [40]. The solid curve is the leading-order HBχPT prediction. The leading-order result describes the data (which have considerable variation themselves) within 15% up to $E_\gamma = 230$ MeV. The difference indicates the size of the higher-order corrections expected of HBχPT and the level of convergence of chiral expansion. Figure 5 shows the differential cross section for $\gamma p \to n\pi^+$ as a function of the pion CM angle. The small angular variation reflects the dominance of the S-wave contribution. Figure 6 shows the differential cross section as a function of the pion Lab angle.

Figure 7 shows A_γ in the total cross section for $\vec{\gamma}p \to n\pi^+$ as a function of photon laboratory energy E_γ. The DDH value of $h_\pi^1 = 4.6 \times 10^{-7}$ is assumed. The asymmetry $A_\gamma(\theta^\pi)$ in the differential cross section for $\vec{\gamma}p \to n\pi^+$ as a function of the pion CM angle is shown in Figure 8 and as a function of the pion Lab angle in Figure 9 ($h_\pi^1 =$

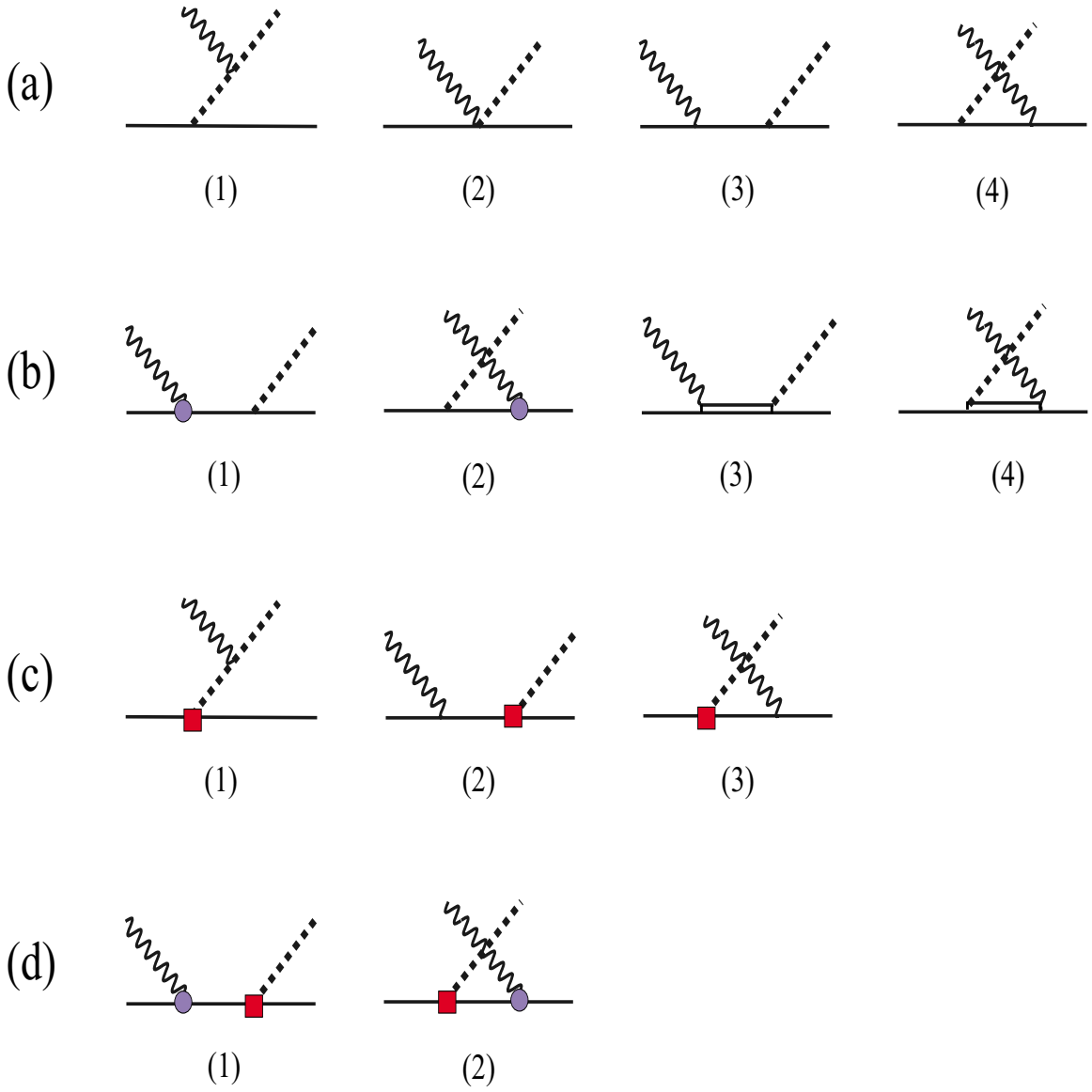

Figure 3: Parity-conserving (PC) leading order (LO) (a) and next-to-leading order (NLO) (b) Feynman diagrams and parity-violating (PV) LO (c) and NLO (d) diagrams for $\vec{\gamma}p \to n\pi^+$. The wavy lines represent the photons, solid lines the nucleons, dashed lines the pions, and the double lines the Δ resonances. The solid circles denote the NLO PC vertices while the squares denote the PV h_π^1 couplings. The groups (b) and (d) are incomplete but sufficient for the purpose of the asymmetry calculation performed in [35].

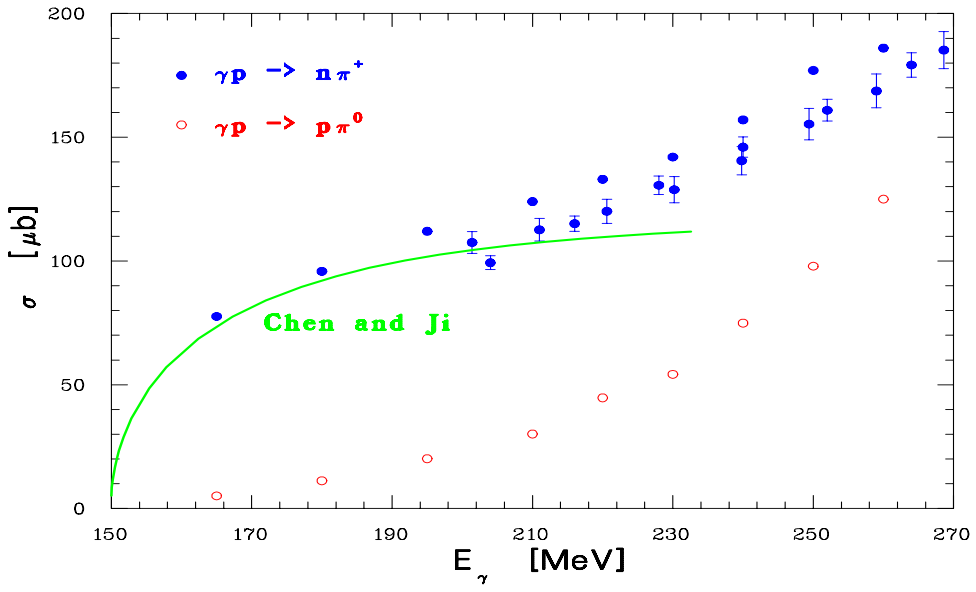

Figure 4: Total cross section for $\gamma p \to n\pi^+$ as a function of photon laboratory energy E_γ. Data points are taken from Reference [40]. The solid curve is the leading-order HBχPT prediction.

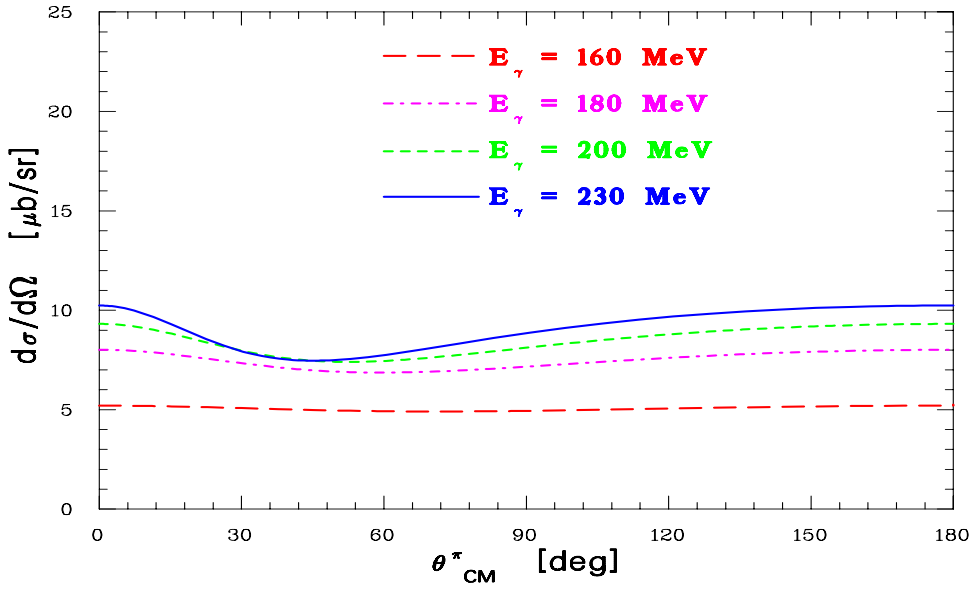

Figure 5: Differential cross section for $\gamma p \to n\pi^+$ as a function of pion CM angle.

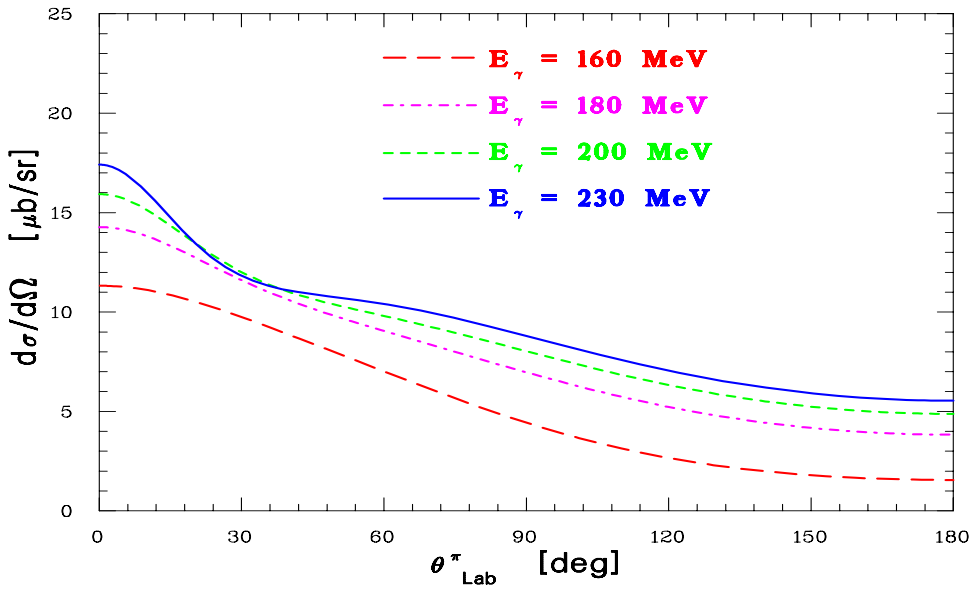

Figure 6: Differential cross section for $\gamma p \to n\pi^+$ as a function of pion Lab angle.

4.6×10^{-7}). Note the strong dominance of the photon polarization asymmetry at forward and backward angles in the threshold region. Only at angles near 90° and $E_\gamma > 200$ MeV does the modification from high partial waves become significant.

2.1 Experimental Considerations

The experiment will take place in Hall A. 400 μA polarized beam will be used to produce a circularly polarized photons by using 10% *r.l.* Cu radiator (see Section 2.4). The electron beam will be deflected away to a local beam dump. The photon beam will be incident on a 80 cm liquid hydrogen target. π^+ will be detected in an ionization chamber detector. The detector will cover the angular range 130°-150°. The expected counting rate is approximately 250 MHz. The ionization chamber will be placed immediately after the magnet of BigBite spectrometer to detect pions in current mode. BigBite will be positioned at a distance of 1.3 m from the target. The choice of the detector type and material was decided after careful studies of background and detector response. Figure 10 shows the proposed experimental setup to study $\vec{\gamma}p \to n\pi^+$.

The experimental conditions are listed in Table 2. The photon beam polarization is very close to the electron beam polarization. For 200 MeV photon, the polarization is 98% of the electron and for 180 MeV photon, the polarization is 93% (see Figure 11). 1000 hours of beam time are required for 20% statistical accuracy. The total systematic uncertainty is anticipated to be smaller.

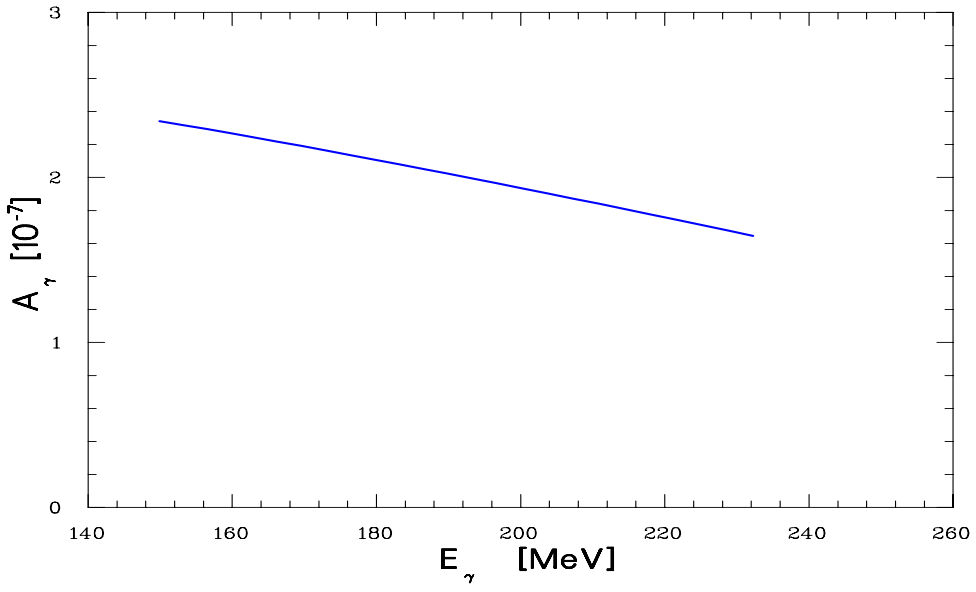

Figure 7: Asymmetry in total cross section for $\vec{\gamma}p \to n\pi^+$ as a function of photon laboratory energy E_γ ($h_\pi^1 = 4.6 \times 10^{-7}$).

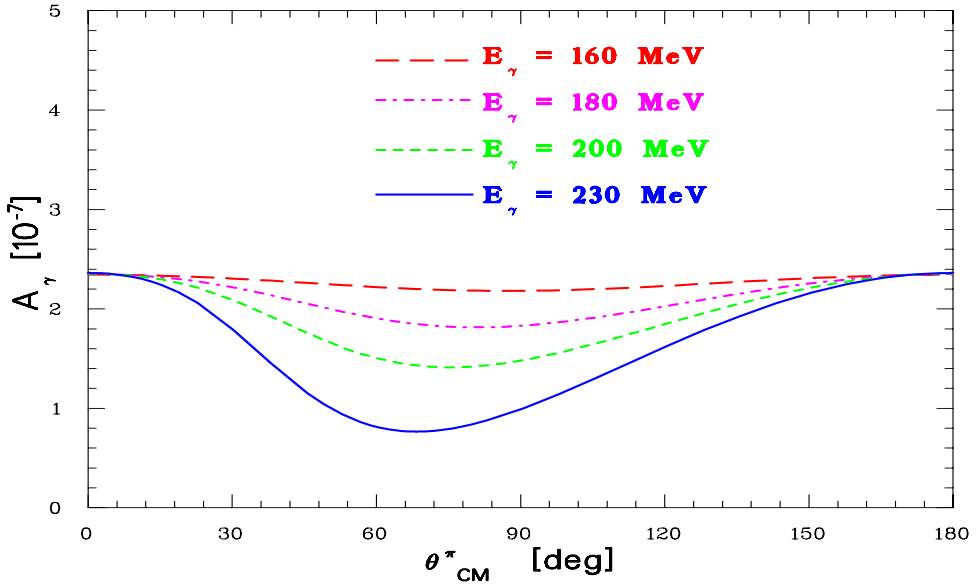

Figure 8: Asymmetry of the differential cross section for $\vec{\gamma}p \to n\pi^+$ as a function of the pion CM angle ($h_\pi^1 = 4.6 \times 10^{-7}$).

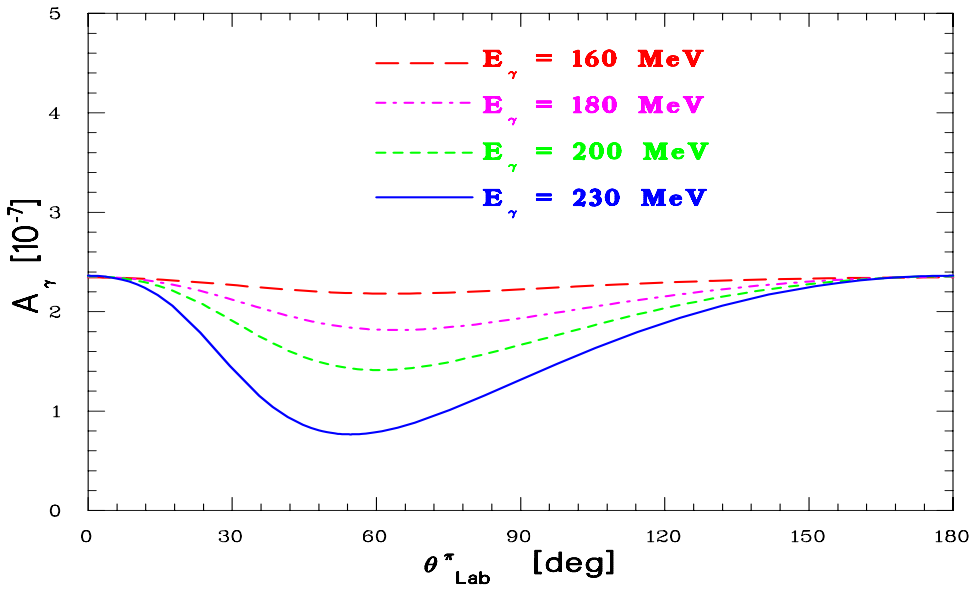

Figure 9: Asymmetry of the differential cross section for $\vec{\gamma}p \to n\pi^+$ as a function of the pion Lab angle ($h_\pi^1 = 4.6 \times 10^{-7}$).

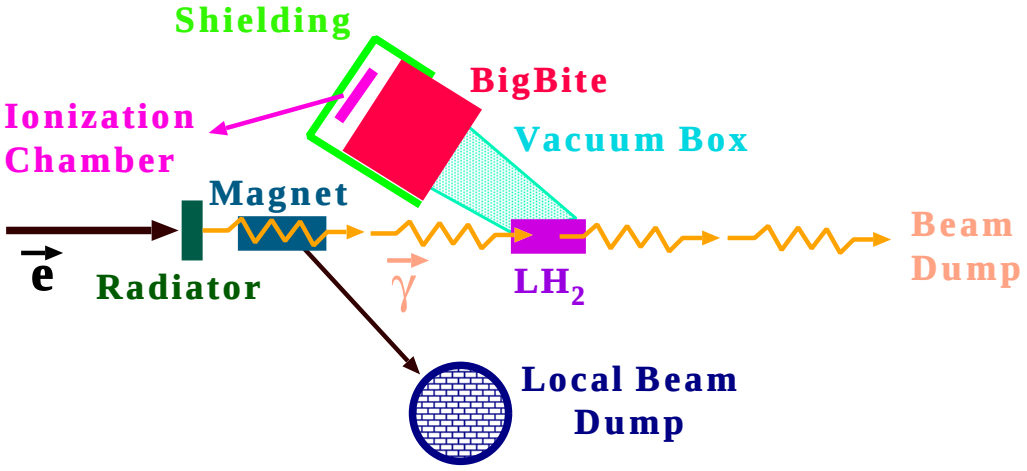

Figure 10: A schematic of the experimental setup in Hall A.

Experimental Hall	**Hall A**
Beam Energy	230 MeV
Beam Current	400 μA
Beam Polarization	80%
Radiator Thickness	10% *r.l.* Cu (0.143 cm)
Photon Energy (E_γ)	230-180 MeV
f (N_γ/N_e)	0.02
Photon Polarization	75%
Target	80 cm LH_2
Luminosity ($\mathcal{L}$)	1.6×10^{38} cm^{-2} sec^{-1}
BigBite Central Angle	140°
Horizontal Angular Acceptance	$\pm 10°$
Vertical Angular Acceptance	$\pm 20°$
Solid Angle Acceptance	0.3 sr
Average Cross Section $\frac{d\sigma}{d\Omega}(\gamma p \to n\pi^+)$	5×10^{-30} cm^2/sr
Theoretical Asymmetry (A_γ)	2.2×10^{-7}
Experimental Asymmetry (A)	$\mathbf{1.7 \times 10^{-7}}$
Statistics Needed for 100% Accuracy ($1/A^2$)	3.7×10^{13}
Time Needed for 100% Accuracy	40 hours
Extra Time (Signal Fluctuations)	25%
Total Time (100% Statistical Accuracy)	50 hours
Total Time (20% Statistical Accuracy)	**1000 hours**

Table 2: Experimental conditions for the proposed measurement.

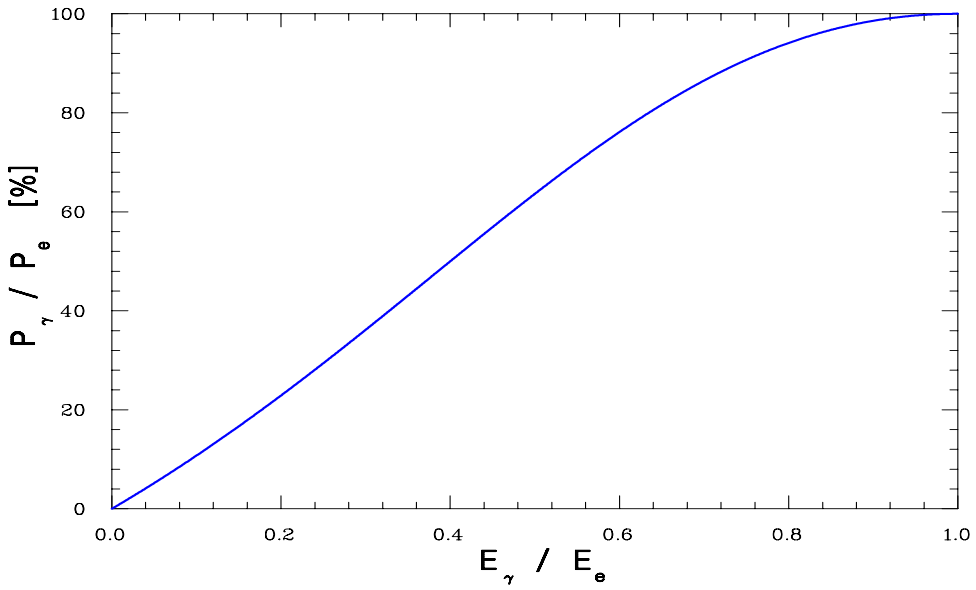

Figure 11: The polarization of the Bremsstrahlung photon as a function of $x = E_\gamma/E_e$ ($P_\gamma/P_e = (4x - x^2)/(4 - 4x + 3x^2)$).

2.1.1 Accelerator and Beam

This experiment requires an electron beam of 400 μA with 80% polarization. The energy of the beam will be 230 MeV. The injector has already produced 550 μA polarized beam with 80% polarization [41]. The accelerator will be able to deliver high quality beam even at this low energy [42]. Note that G0 is already approved to run at 335 MeV [43]. The requirements on the beam quality are the same as the already approved parity experiments at JLab.

It is unlikely that any other experimental hall can run a physics program with such low energy. However, often only two halls are taking data anyway. Sometimes only one hall is taking data. This experiment could run when one or both of the other two halls are open for maintenance. When only one hall is running, the accelerator availability is much greater than 50% which implies that this experiment could be scheduled for less calendar days than usual. Every thing needed to successfully run this experiment is available and has either been tested already in Hall A or can be easily modified to accommodate this experiment.

The beam instrumentations such as beam intensity and position will be tested at the proposed current. It is usually the case that the larger the values of the beam signals, the smaller the intrinsic errors. Møller polarimeter will be used to measure the beam polarization. We will not use the Compton polarimeter because of the low beam energy.

2.1.2 Hall A

Hall A is the ideal place for this experiment. The BigBite spectrometer (magnet, detectors, and electronics) will be available for this and other experiments. There will be major work in the target area to install the septum magnets so part of the requirements for this experiment can be satisfied easily. HAPPEX [44] already installed and used the DAQ and the beam control devices. Thus we are only left with one major equipment installation (the local beam dump). In conclusion, it is easier to install this experiment in hall A than in hall C.

2.1.3 Radiator

A 10% Cu radiator will be used to generate the photon beam. A water cooling system will be used to dissipate the heat deposited in the radiator foil by the electron beam. The beam will be rastered on the radiator and the cooling system will be capable of removing the high heat load required by this experiment [45]. The Hall A beamline is already equipped with a radiator. The radiator is currently located at 74 cm upstream of the target. The radiator will be moved 126 cm further upstream to make space for the sweeping magnet. The required foil thickness will be added to the radiator ladder. The electron energy loss in the radiator will be approximately 3 MeV. The heat deposited in the radiator will be 1200 W for 400 μA beam current. Local shielding will be put around the radiator.

Due to Coulomb multiple scattering, the electron beam after traversing the radiator will have an angular distribution with a width given by:

$$\theta_0 = \frac{13.6 \ [\mathrm{MeV}]}{\beta \, pc} \sqrt{0.1} = 17 \text{ mr} \ \ (= 1.0^\circ) \ , \tag{9}$$

while the angular distribution of the photon beam has a smaller characteristic angle. The photon beam will have 1.0° clearance all the way to the standard hall A beam dump. Photons with angles greater than 1.0° will be collimated. The angular distribution of the electrons after the radiator and of the photons produced in the radiator are shown in Figure 12 for electron and photon energies greater than 100 MeV.

The interaction of the electron beam with the radiator was simulated using GEANT [46]. The angular and energy distribution of the photons produced in the radiator are shown in Figure 13.

2.1.4 Sweep Magnet

A dipole magnet will be used to deflect the beam to a local beam dump. For a 45° deflection of 230 MeV electron beam, a 0.6 T.m magnet is needed (such magnet is available on site). The angular and energy distribution of the electrons after the radiator are shown in Figure 14.

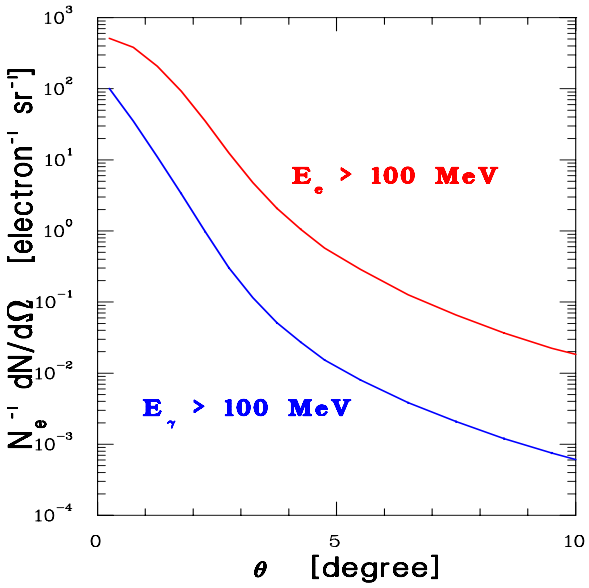

Figure 12: The angular distribution of the electrons after the radiator and of the photons produced in the radiator for electron and photon energies greater than 100 MeV.

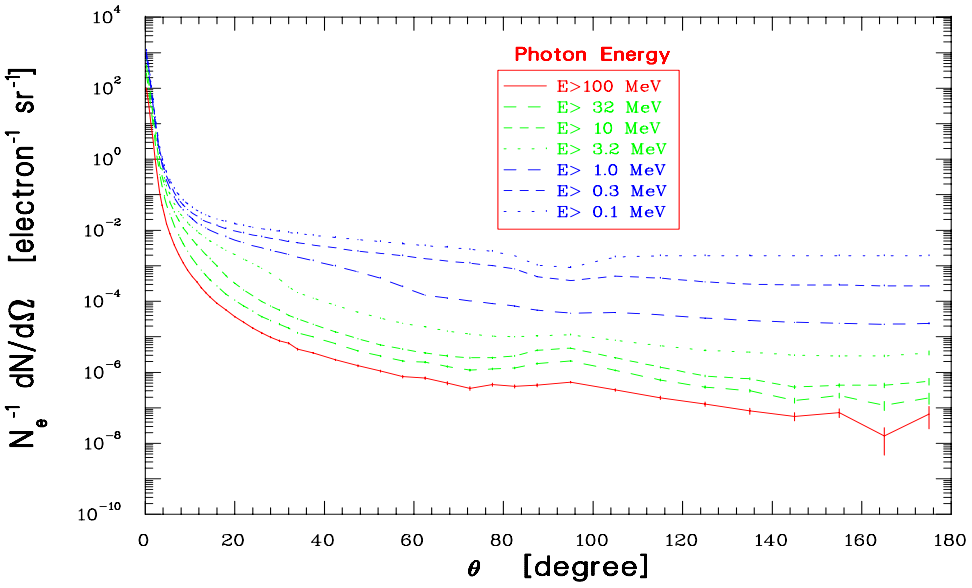

Figure 13: The angular and energy distribution of the photons produced in the radiator.

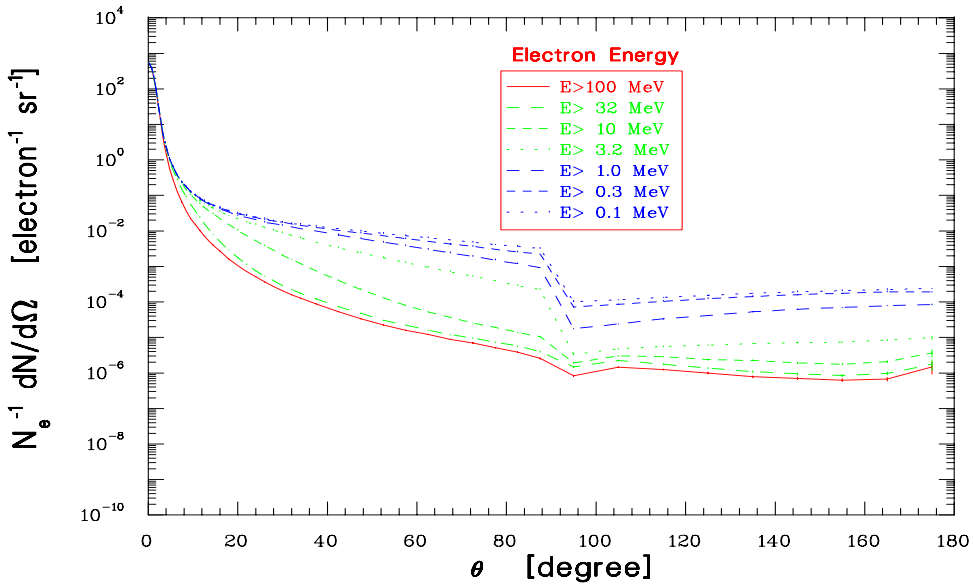

Figure 14: The angular and energy distribution of the electrons after the radiator.

2.1.5 Local Beam Dump

With a 10% radiator, the low energy beam will be very spread out, too much so to reach the standard hall A beam dump. A low power dump (total beam power is 92 kW) will be mounted much closer to the target. Dump location would depend on shielding between the dump and the detector. Although this is a major equipment requirement, the design and construction of such beam dump is possible [41]. Recently, a 15 kW local beam dump was used during an experiment in Hall C [47].

2.1.6 Scattering Chamber

The current scattering chamber has a radius of 0.55 m. The scattering chamber (and target) will be pushed upstream 80 cm to install the septum magnets in the Fall of 2001 (see Figure 28). When the chamber is in this position it will be easier to place BigBite magnet closer to the target at backward angles. Most likely we will be able to run while the hall is in this configuration. Running with the current position of the scattering chamber is also possible. We will need to rebuild the scattering chamber to meet the requirements of this experiment.

2.1.7 Target

This experiment will use the Hall A liquid hydrogen target. The target thickness will be 80 cm. The operating temperature will be 19 K and the operating pressure will be 25 psi. The target density will be 0.072 g/cm^3. A new cell block will be designed to hold the

hydrogen cell. This cell block will have full clearance for the photon beam and the pions [48].

The cell will be approximately 8 cm in width and 8 cm in height. Most of the photon beam will pass through the target (99.7% of photons will pass through a circle with a diameter of 5 cm). All surrounding materials, including target walls, flanges and other structures, including the interaction chamber walls, exit pipes and flanges, must be outside the photon beam envelope. The target will require about 100 W of cooling power.

2.1.8 Beam Exit Pipe

Only the first part of the beam exit pipe must be modified to allow the photon beam to reach the standard hall A beam dump. The part connecting the scattering chamber to the first flange will be replaced to increase its diameter. The current exit beam pipe is designed for 25 mr (1.5°) beam envelope. All the Hall A equipment will be placed at angle greater than 90° to protect it from radiation.

2.1.9 Vacuum Box

A vacuum box made of Aluminum will connect the scattering chamber to the pion detector (see Figure 30).

2.1.10 BigBite Spectrometer

BigBite spectrometer [49] will be used to detect the π^+. This spectrometer is characterized by a large solid angle acceptance combined with a very large momentum acceptance (200-900 MeV/c). The spectrometer consists of a single dipole magnet followed by a detector package. BigBite will be placed at about 1.3 m from the target to provide a larger solid angle acceptance. To increase the solid angle further, the opening horizontal gap will be increased from 25 cm to 60 cm. This will be possible since the two pieces of the magnet are bulleted together. The momentum acceptance will be (50-200 MeV/c). The spectrometer central angle will be 140°. The flight path from the target to π^+ detector will be $\sim$2 m. BigBite magnet with the described configuration is shown in Figure 29.

BigBite, shown in Figure 15, is equipped with two wire chamber packages for tracking, a scintillator, and Čerenkov for particle identification. A new detector package will be installed by another proposed experiment [50]. In order to shield the target area from the fringing field of the magnet, a field clamp has been employed. The ionization chamber will be placed at the front of the detector package. The magnet will be energized so the spectrometer will accept particles with momenta between 50-200 MeV/c. Figure 16 shows π^+ momentum in the laboratory frame as a function of photon laboratory energy E_γ for $\theta^\pi_{Lab} = 140°$. During production running, all other detectors will be turned off. At the beginning of the experiment, the detectors will be turned on and the beam current will be lowered to 1 μA to study the distributions and identities of the particles detected. Data will be taken also with magnet field set to zero and to its maximum to study the neutral background. The production data will be taken with a magnet setting of (50-200 MeV/c),

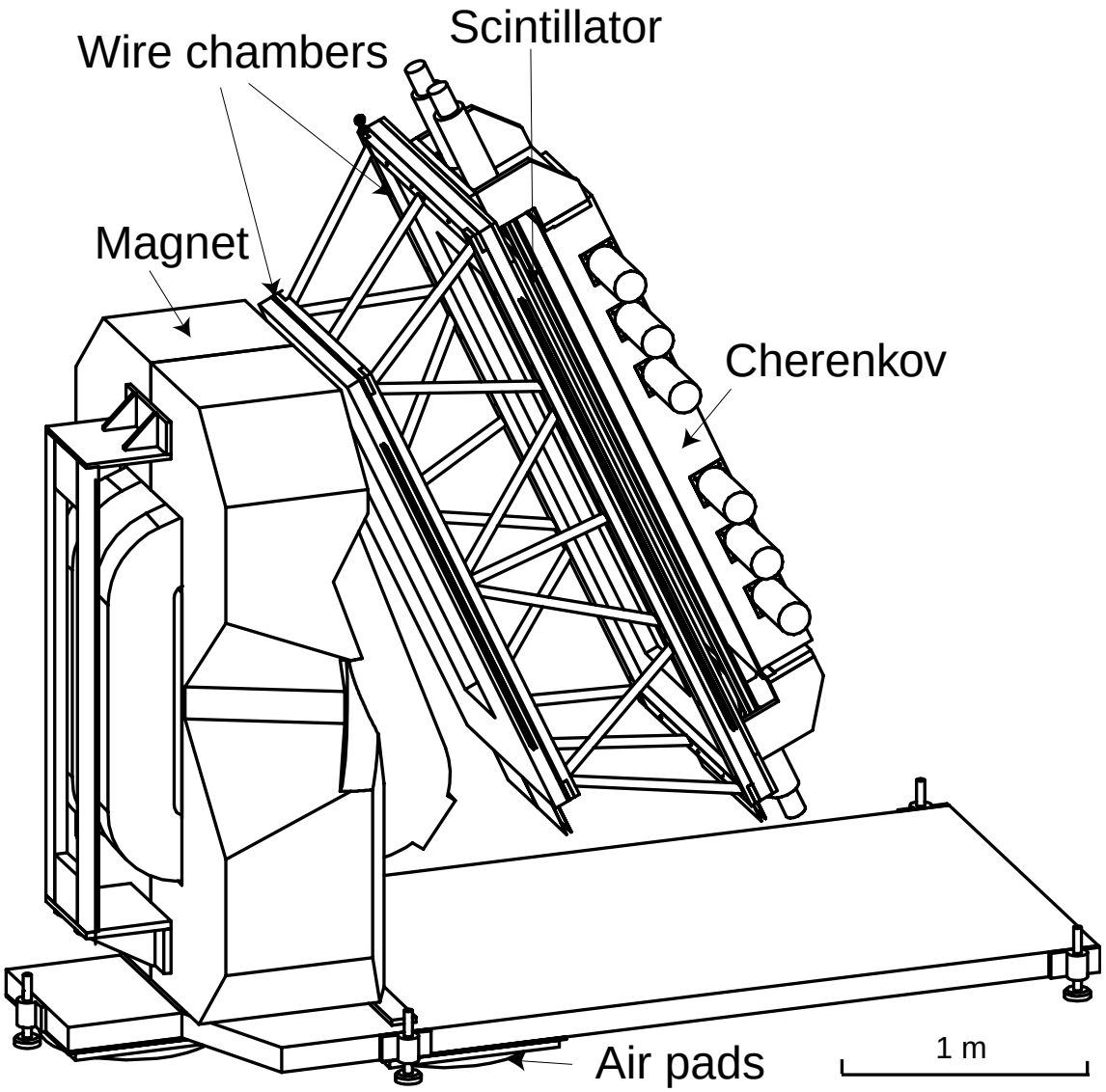

Figure 15: BigBite spectrometer in its original configuration at NIKHEF. BigBite is equipped with two wire chamber packages for tracking, a scintillator, and Čerenkov for particle identification. In order to shield the target area from the fringing field of the magnet, a field clamp has been employed. A new detector package will be installed by another proposed experiment [50].

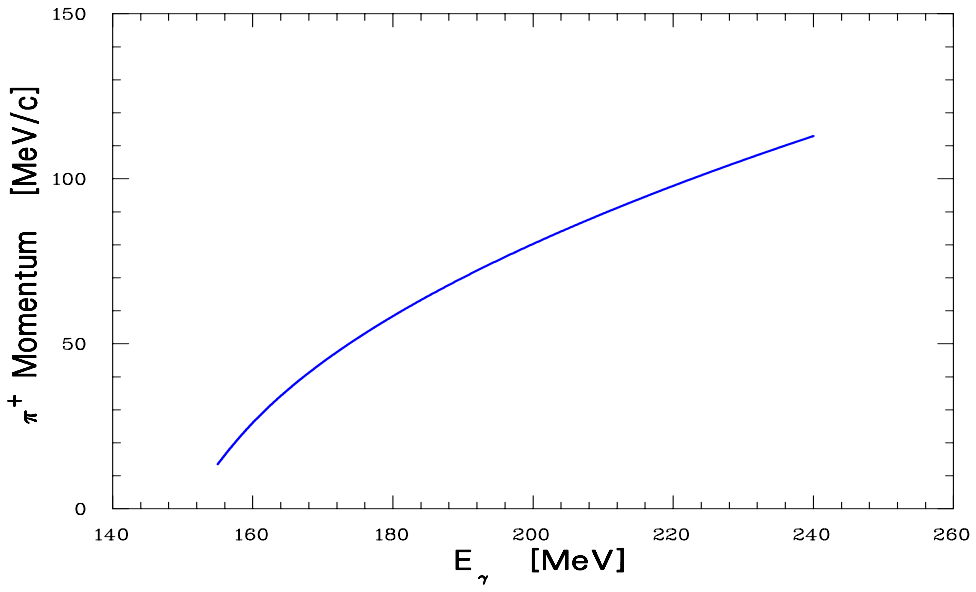

Figure 16: π^+ momentum in the laboratory frame as a function of photon laboratory energy E_γ for $\theta^\pi_{Lab} = 140^\circ$ ($\theta^\pi_{CM} \sim 152^\circ$).

BigBite spectrometer (magnet, power supply, detector package, and electronics) has been brought from NIKHEF to JLab and is now stored in Hall A. BigBite will be connected to the scattering chamber using a vacuum box. Similar configuration of BigBite will be used by another proposed experiment [50].

BigBite magnet with the above configuration was studied using SNAKE simulation [51]. The results indicate that the magnet will meet the specified requirements (solid angle and path length). The simulations also indicate that the detection area will be approximately 1 m^2.

2.1.11 π^+ Ionization Chamber Detector

An ionization chamber (gain = 1) at the back of BigBite magnet will be used to detect π^+ (see Figure 30). The area of the chamber is expected to be 1 m^2 with a thickness of 3 cm. A detailed simulation study will be done to determine the geometry, segmentation, and thickness of the ionization chamber. The detector will be readout in integration mode similar to the HAPPEX experiment [44]. The detector rate is expected to be 250 MHz. The ionization chamber was chosen because it is the least sensitive to neutral background [52]. GEANT simulation shows that he ionization chamber efficiency is about 10^{-3} for low energy photons.

The response of the ionization chamber is very linear. For minimum ionizing particles ($dE/dx = 2.44$ keV/cm), the primary number of ion-pairs for Argon gas is $n_p = 30$ ion-pairs per cm and the total ionization is $n_T = 94$ ion pairs per cm [53]. Figure 17

shows the number of ion-pairs produced in the ionization chamber by pions produced in the target with momenta 60-110 MeV/c. If the pion decays on its way to the detector, the muon will be in a cone symmetric around the original pion direction, its signal is also shown in the figure. For 250 MHz pion rate, the current output of the ionization chamber with a thickness of 3 cm will be ∼20 nA.

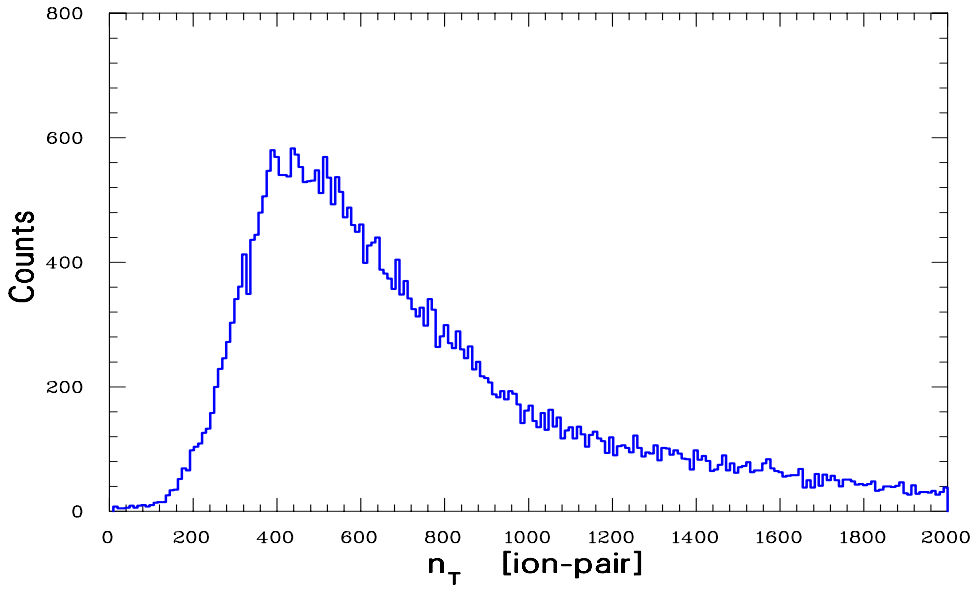

Figure 17: The number of ion-pairs produced in the ionization chamber by pions produced in the target with momenta 60-110 MeV/c.

High energy tails are cause for concern. Fluctuations in the number of primary ion pairs will result in a non-zero resolution which adds in quadrature to the statistical error according to:

$$\Delta A = \sqrt{\frac{1}{N}(1+r^2)}\ , \tag{10}$$

where N is the number of incoming pions and $r = \Delta n/n$. A bad resolution results in a longer running time to achieve the same accuracy. Statistical fluctuations in the ionization chamber is expected to increase the running time by 25%.

2.1.12 Data Acquisition

We will use the same data acquisition system as used during the HAPPEX experiment [44]. The pion signal in the ionization chamber will be read in current mode.

Reaction	Parity-Violating
$\vec{\gamma}p \to p\pi^0$	no
$\vec{\gamma}p \to \gamma p$	yes
$\vec{\gamma}e \to \gamma e$	yes
$\vec{\gamma}A \to e^+e^-$	yes

Table 3: Summary of the background reactions.

2.2 Detector Backgrounds

Table 3 lists the relevant background channels. One source of background is π° photoproduction which has a cross section comparable to π^+ (see Figure 4). Another source of background will be Compton scattering off the electrons, $\vec{\gamma}e \to \gamma e$. Most of the background is expected to be low energy forward going particles. The spectrometer will be set to detect particles with momenta greater than 50 MeV/c and at a backward angle of 140° which will help in reducing the charged particles background.

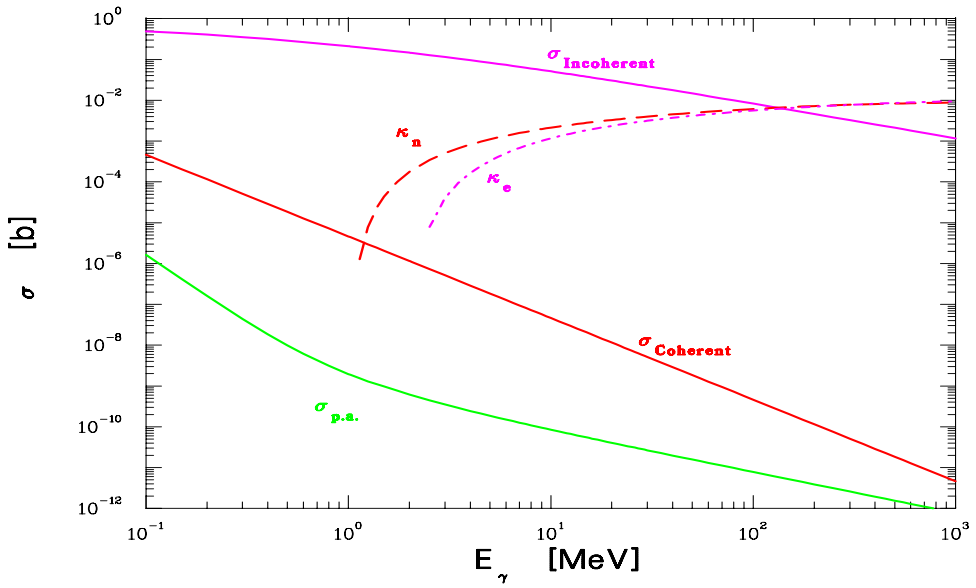

Figure 18: Photon total cross section as a function of energy in LH_2, showing the contributions of different processes [54].

The contributions of different processes to the photon total cross section as a function of energy in LH_2 is shown in Figure 18 [54]. These processes are:

$\sigma_{p.a.}$	:	Photon absorption
σ Coherent	:	Rayleigh scattering
σ Incoherent	:	Compton scattering off an electron
κ_n	:	Pair production, nuclear field
κ_e	:	Pair production, electron field.

The interaction of the photon beam, produced at angle $< 1.35°$ in a 10% Cu radiator by 400 μA electron beam, in a 80 cm LH_2 target was studied in GEANT. The results are shown in Figures 19-23 where the rate in a solid angle of 0.3 sr is plotted as a function of angle. The vertical lines indicate the angular acceptance of BigBite.

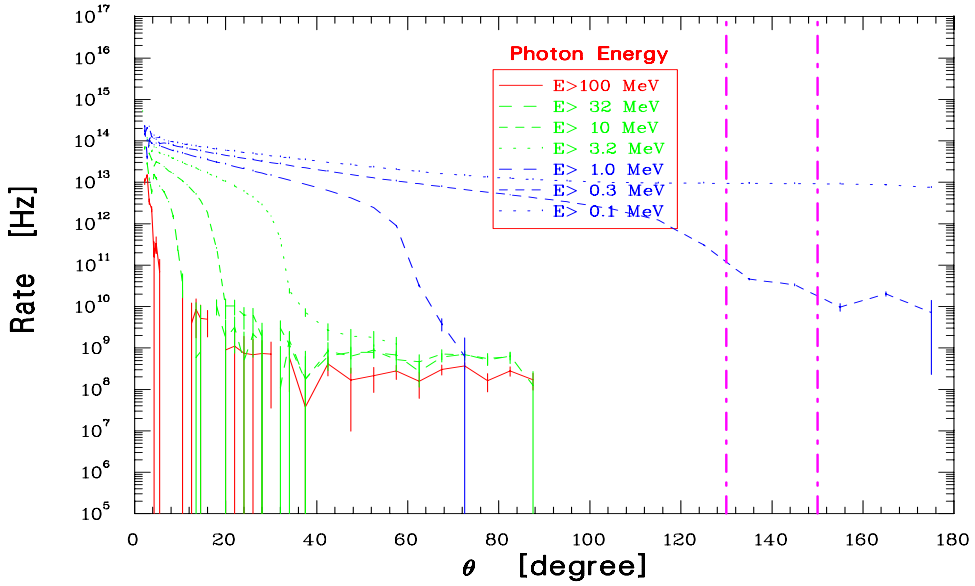

Figure 19: The angular and energy distribution of the photons produced by the photon beam in the target.

2.2.1 Photons and π^0 Background

$\vec{\gamma}p \to p\pi^0$ is parity-conserving. The A_γ asymmetry in $\vec{\gamma}p \to \gamma p$ proton Compton scattering was calculated in Reference [55] to be $\ll 10^{-8}(E_\gamma/70\,[\mathrm{MeV}])^3$. The A_γ asymmetry in $\vec{\gamma}e \to \gamma e$ electron Compton scattering was calculated in Reference [56] to be of order:

$$\frac{\alpha m_e^2}{2\pi M_W} \sim 10^{-13} \ . \tag{11}$$

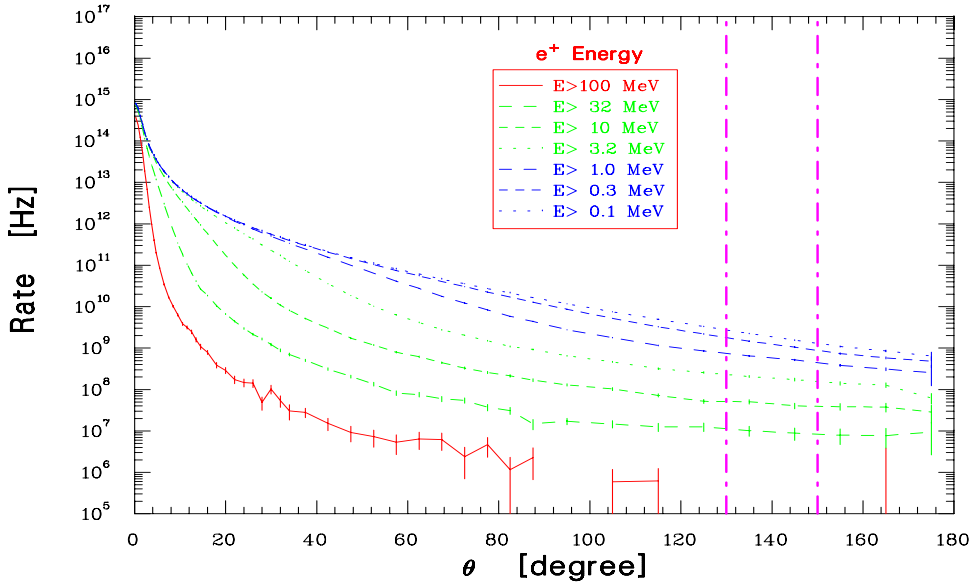

Figure 20: The angular and energy distribution of the e^+ produced by the photon beam in the target.

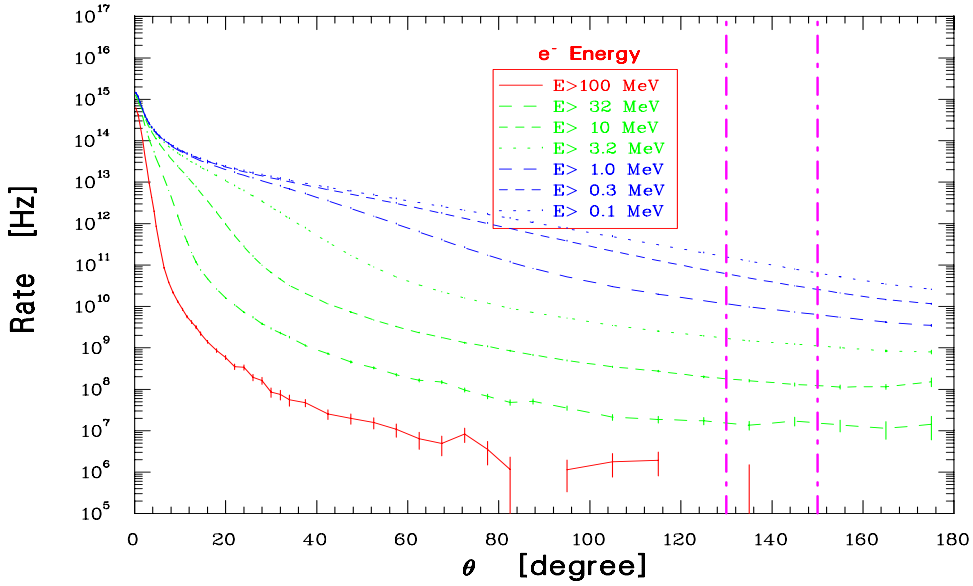

Figure 21: The angular and energy distribution of the e^- produced by the photon beam in the target.

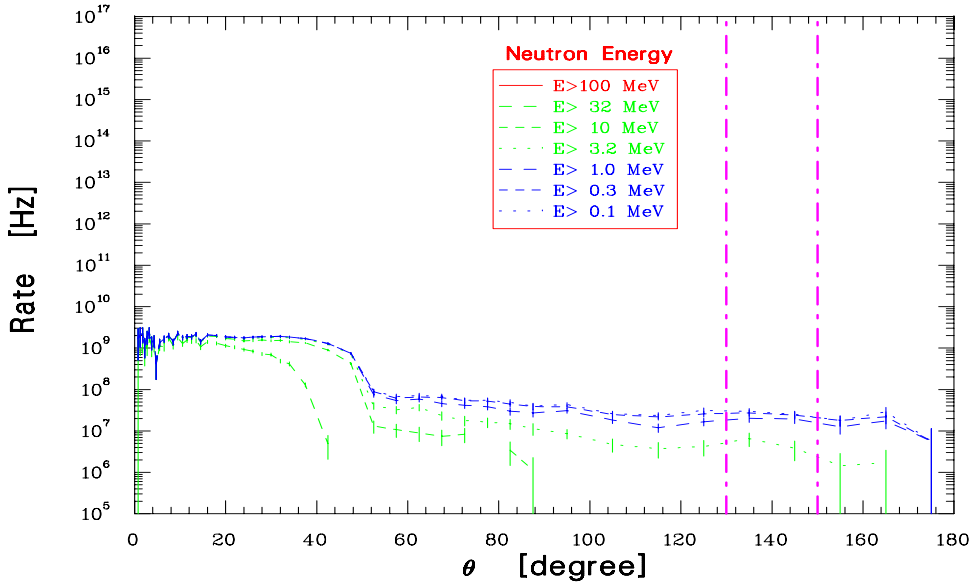

Figure 22: The angular and energy distribution of the neutrons produced by the photon beam in the target.

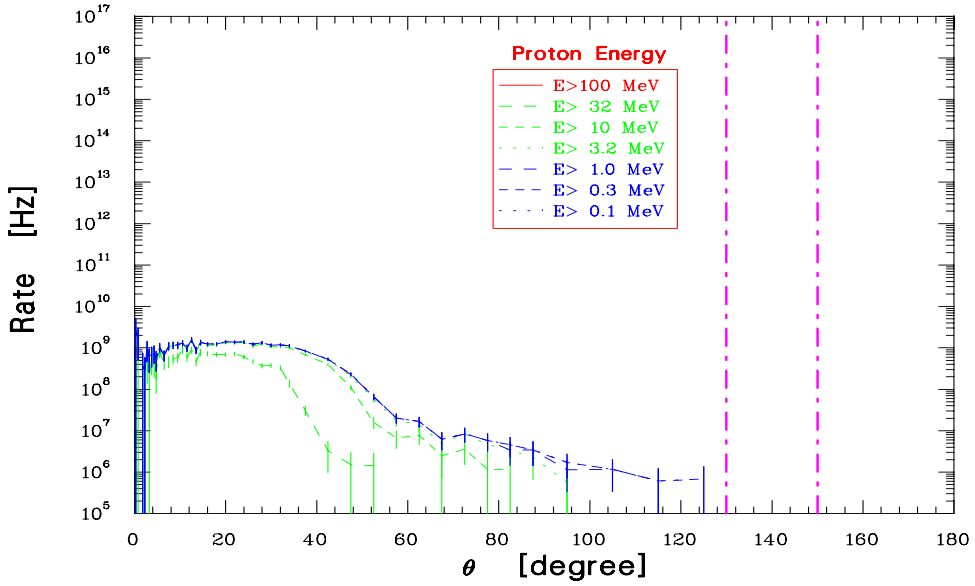

Figure 23: The angular and energy distribution of the protons produced by the photon beam in the target.

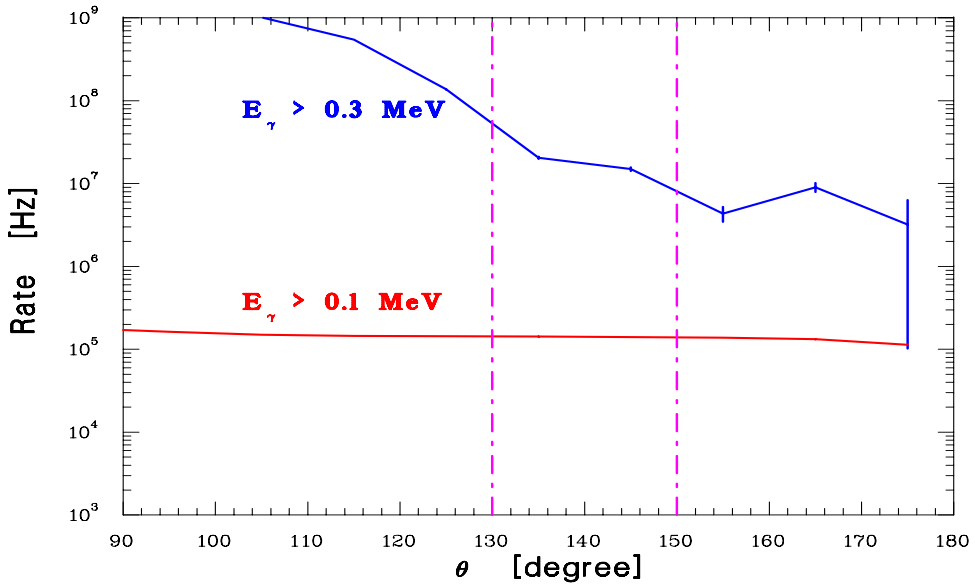

Figure 24: The rate of low energy photons in the ionization chamber assuming lead shielding of 2 g/cm^2 and detection efficiency of 10^{-3}.

The backward photons with energies $\lesssim$0.3 MeV, shown in Figure 19, are the product of Compton scattering off the electrons in the target by the photon beam (their energy can not be larger than $m_e/1.8$). We will use a 2 g/cm^2 sheet of lead between the target and the magnet to shield these photons. Figure 24 shows the rate of these low energy photons in the ionization chamber when a lead shielding of 2 g/cm^2 and a detector efficiency of 10^{-3} were used.

Approximately, 20 MHz of photons with energy $\lesssim$0.3 MeV will give signal in the detector. GEANT simulation of the response of the ionization chamber to these photons is shown in Figure 25. The effect of this background will be a dilution of the asymmetry of about 10%.

2.2.2 e^+e^- Pair Production Background

The e^+e^- pair production by photons is parity-violating. The A_γ asymmetry in $\vec{\gamma}A \to e^+e^-$ pair production is estimated to be of the order $\frac{G_F}{\sqrt{2}}\frac{Q^2}{2\pi\alpha} \sim 10^{-4}m_e^2 < 10^{-10}$. The electron and the positron in the pair produced by the photon beam will be polarized at some level with a polarization that will flip with the photon helicity flip. Their degree of polarization depend on their energy and angle [57]. The vacuum box will reduce the magnet pole tip scattering. e^- will be swept away by the magnet. GEANT simulation shows that the e^+ rate is $\lesssim$2 MHz (see Figure 20) which will dilute the measured asymmetry by 1%.

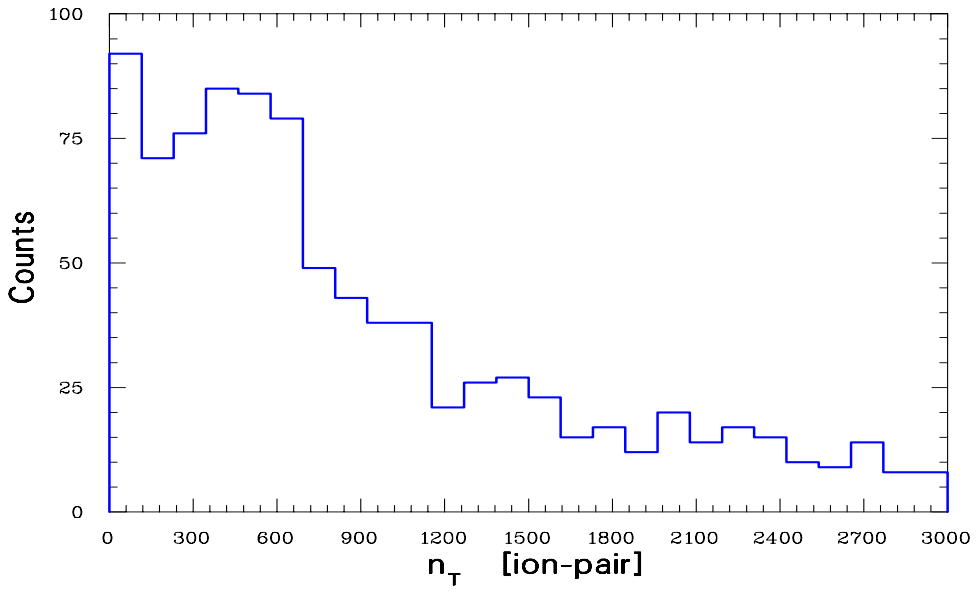

Figure 25: GEANT simulation of the response of the ionization chamber to 0.3 MeV photons.

2.2.3 Target Windows Background

The main background from the target windows will be the production of π^+. The total thickness of the entrance and exit windows of the target cell will be approximately 0.1 cm of Aluminum. The π^+ production off the windows is estimated to be equal to the ratio of protons in windows compared to protons in the target. The windows will contribute on the level of 3%. We assume here that the asymmetry is the same as in the case of a free proton (no modification in the nuclear medium).

2.2.4 Neutron Background

The ionization chamber is insensitive to neutrons. Shielding will be placed around the detector, radiator, and local beam dump to reduce the neutron background in the hall. The neutron flux from the radiator is very large as can be seen in Figure 26.

2.2.5 Pion Decay

The flight path from the target to π^+ detector will be $\sim$2 m. For 100 MeV/c pions ($c\tau$ = 7.8 m, $\pi^+ \rightarrow \mu^+\nu_\mu$), 70% will survive to reach the detector. Most of the muons ($c\tau$ = 659 m) will make it to the detector so they will be counted. The muon momentum is 30 MeV/c when the pion decays at rest.

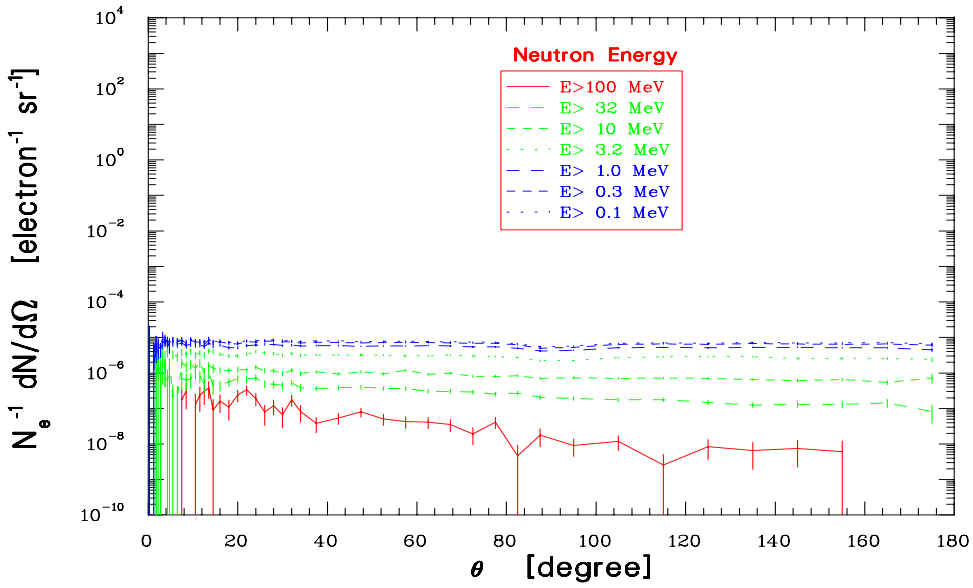

Figure 26: Neutron flux from the radiator. Shielding will be placed around the detector, radiator, and local beam dump to reduce the neutron background in the hall.

2.2.6 Summary of the Detector Backgrounds

Source of Background	Dilution Effect
Photons	10 %
e^+	1%

Table 4: Summary of the detector background.

There are only two background contributions in the detector: photons with energy $\lesssim$ 0.3 MeV and e^+ with energy greater than 50 MeV. Since the parity-violating asymmetries of the backgrounds are much smaller than the measured physics asymmetry, the only effect these backgrounds have is to dilute the physics asymmetry. Table 4 summarizes the detector backgrounds and their dilution effects.

2.3 Systematic Errors

2.3.1 Helicity Correlated Beam Parameters

The systematic uncertainty due to the beam parameters is anticipated to be smaller than the statistical uncertainty. During the 1999 HAPPEX run the corrections due to beam parameters were in the worst case $\sim 5 \times 10^{-8}$. The situation will be much improved for future parity experiments at JLab. HAPPEX II [58] will measure an asymmetry to a total systematic error of 3×10^{-8} (only 1×10^{-8} is due to the beam false asymmetries). The conditionally approved parity lead radius experiment will measure an asymmetry of $\sim 5 \times 10^{-7}$ to a systematic error $\leq 1 \times 10^{-9}$ [59]. Further, for these two experiments the systematic errors are dominated by the uncertainty in measuring the beam polarization. Thus we conclude that the systematic errors due to the injector, beam parameters, and DAQ are small. The error in measuring the beam polarization for this experiment is only 3%.

The requirements on the relative precision on the beam parameters (energy, angle, and position) are much less stringent than the other parity experiments because the cross section is very insensitive to beam energy and scattering angle (see Figure 6). The helicity correlated beam position differences will be measured and corrected.

We will use photon intensity monitors to measure and control the photon beam intensity and correct for fluctuations. One possibility is to use Čerenkov detector as a photon intensity monitor. The fluctuations in intensity due to differences in beam position are expected to be very small since only the far tails of the photon beam are collimated.

2.3.2 Parity Violation in Electron Bremsstrahlung

The parity violation in polarized electron bremsstrahlung caused by electroweak interference and weak NN interactions was calculated in Reference [60]. The order of magnitude of the effect is determined by the parameter:

$$\rho = \frac{G_F}{\sqrt{2}} \frac{Q^2}{2\pi\alpha} \ . \tag{12}$$

In the forward direction and near the maximum of the bremsstrahlung, the parameter ρ is very small ($< 1 \times 10^{-9}$). Thus, the change in the intensity of the photon beam is negligible.

2.3.3 Linearly and Circularly Polarized Photon Beam

The Bremsstrahlung photon polarization from high energy electrons with arbitrary polarization was studied in Reference [61]. It was found that while Bremsstrahlung is both linearly and circularly polarized (elliptic polarization), the linear polarization is independent of any polarization of the initial electron and circular polarization occurs only for polarized initial electrons. The over all linear polarization of photons produced in a radiator by incoherent Bremsstrahlung vanishes upon integration over all the outgoing

Bremsstrahlung cone [62]. The helicity-correlated beam motion could produce a residual linear photon polarization. The contribution of the Σ asymmetry is estimated to be $< 1 \times 10^{-9}$.

2.3.4 Polarized Protons in the Target

Due to the presence of magnetic field in the target area, the proton polarization in the target is approximately:

$$P = \frac{\mu_p B}{k T} \ . \tag{13}$$

For 19 K, $P \sim 5 \times 10^{-5}$/T. The double polarization asymmetry, $(\sigma_{3/2} - \sigma_{1/2})/(\sigma_{3/2} + \sigma_{1/2})$, for pion photoproduction in the proposed photon energy region is approximately -1. The fringe field from BigBite magnet in the target area will be kept below 2 Gauss. The nominal field of the magnet for this experiment will be 0.3 T. A field clamp will be used to shield the target area from the fringing field of the magnet. The systematic error associated with polarized protons in the target is estimated to be 4%.

2.3.5 Magnet Pole Tip Scattering

A vacuum box made of Aluminum will be used to connect the scattering chamber to the detector package. All charged particles have such low energy that when hitting the walls of the vacuum box, they will be stopped. Therefore, there will be no re-scattering from a magnetized iron (note that the pions are spinless particles).

Magnet pole tip scattering could produce helicity-dependent intensity of the low energy photon background in the ionization chamber. These photons, where most of the background comes from, have very low polarization. The photons could re-scatter from the magnetized iron in the magnet to produce helicity-dependent intensity in the detector. Estimates show that this should be very small with the use of the sheet of lead and the vacuum box.

2.3.6 Summary of the Systematic Errors

Source	Asymmetry	Contribution
Helicity Correlated Beam Fluctuations	1×10^{-8}	6%
Beam Polarization		3%
Polarized Protons in the Target	0.7×10^{-8}	4%

Table 5: Summary of the systematic errors in this experiment. A total systematic error of less than 10% is expected

The systematic errors specific to this experiment are related mainly to the fact that we are detecting pions in our special detector and to the use of the radiator. Since π^+ is emitted in an S-wave and has spin zero, this prevents any of the photon helicity from leaking directly into the pions. The systematic errors due to detector background are small as discussed in the previous section. The systematic errors in this experiment are summarized in Table 5. A total systematic error of less than 10% is expected.

2.4 Radiation Budget

The running conditions for this experiment: 400 μA of 230 MeV beam on 10% radiator, raise the issue of radiation produced in the hall (both the instantaneous and the integrated radiation. Preliminary calculations done by the Radiation Control Group (RCG) [63] show that this experiment would meet all the requirements including the site boundary annual design goal limit. The RCG recommended using local shielding around the radiator. Shielding will also be placed on top of the radiator to stop the neutrons from penetrating the roof of the hall. Adequate shielding must be put also around the local beam dump.

3 Beam Time Request

We request the following beam time:

- 24 hours for the accelerator to establish 230 MeV in Hall A. This time will be scheduled during machine development period as early as possible.
- 8 hours for background and radiation studies and detector calibration.
- 8 hours for the accelerator to establish 230 MeV in Hall A at the beginning of data taking.
- 40 hours for background and radiation studies and for detector calibration.
- 1000 hours for production running.

The total request of beam time is 1080 hours (or 45 days).

4 Summary

Measurement of parity-violating effects have received much attention in recent years. The $\Delta S = 0$ non-leptonic weak interaction is the last sector of the weak interaction where the main aspects of the electroweak theory are not presently verified. The asymmetry in pion photoproduction will be measured to statistical an accuracy of 20%. This would determine the weak pion-nucleon coupling constant on the same level of accuracy in a reasonable beam time.

Although this experiment and the LANSCE experiment will measure the same coupling constant, these two experiment are completely different: The reaction each used to measure this constant is different, the experimental procedures are different, and the theoretical approaches are also different. These two experiments measuring the same quantity to approximately similar error bar would have a major impact in the nuclear physics. Figure 27 shows the projected error bar compared to other experiments. We ask for the PAC full support to enable this experiment to be scheduled in short period of time.

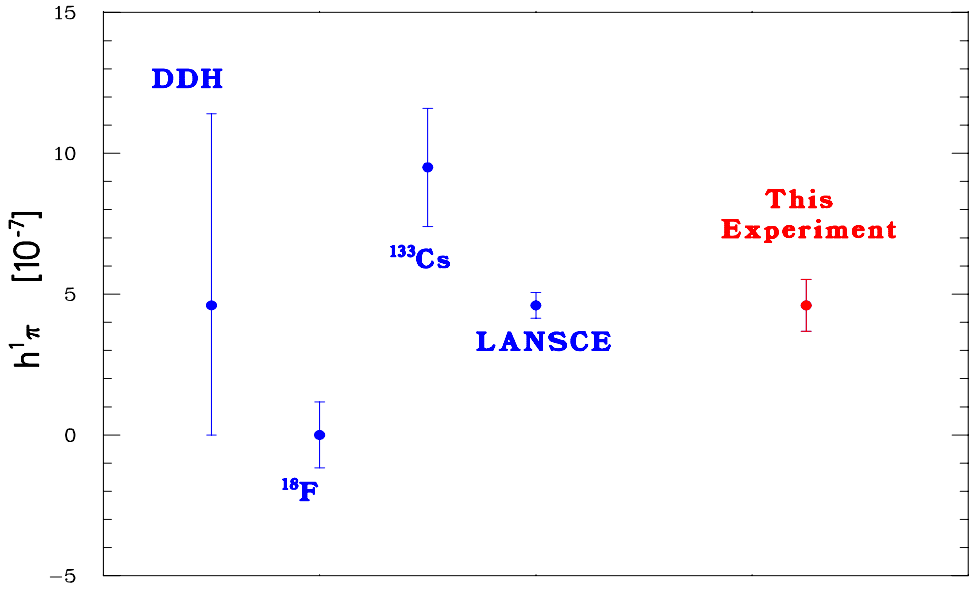

Figure 27: Values of h^1_π from (left to right) DDH theoretical estimate, ^{18}F experiments, ^{133}Cs experiment, and expected statistical uncertainty from LANSCE experiment (it will achieve this uncertainty in 9 months of data taking). The last value represents the expected statistical uncertainty from this experiment in 1.5 months of data taking.

5 Acknowledgment

We are specially grateful to Jiunn-Wei Chen and Xiangdong Ji from University of Maryland for their most valuable theoretical calculations. We gratefully acknowledge the help from Pavel Degtyarenko for providing GEANT simulations.

References

[1] C. S. Wu *et al.*, Phys. Rev. **105**, 1413 (1957).

[2] T. D. Lee and C. N. Yang, Phys. Rev. **104**, 254 (1956).

[3] R. P. Feynman and M. Gell-Mann, Phys. Rev. **109**, 193 (1958).

[4] S. Weinberg, Phys. Rev. Lett. **19**, 1264 (1967).

[5] N. Tanner, Phys. Rev. **107**, 1203 (1957).

[6] V. M. Lobashov *et al.*, JETP Lett. **5**, 59 (1967); Phys. Lett. **B25**, 104 (1967).

[7] B. Desplanques, J. Donoghue, and B. R. Holstein, Ann. Phys. **124**, 449 (1980).

[8] B. R. Holstein, Phys. Rev. **D23**, 1618 (1981).

[9] W. Haeberli and B. R. Holstein, nucl-th/9510062.

[10] B. Desplanques, Phys. Rep. **297**, 2 (1998).

[11] V. M. Dubovik and S. V. Zenkin, Ann. Phys. **172**, 100 (1986).

[12] G. B. Feldman, G. A. Crawford, J. Dubach, and B. R. Holstein, Phys. Rev. **C43**, 863 (1991).

[13] E. G. Adelberger and W. C. Haxton, Ann. Rev. Nucl. Part. Sci. **35**, 501 (1985).

[14] B. Desplanques, nucl-th/0006065.

[15] E. M. Henley, W-Y. P. Hwang, and L. S. Kisslinger, Phys. Lett. **B367**, 21 (1996); errata, ibid. **B440**, 449 (1998).

[16] D. B. Kaplan and M. J. Savage, Nucl. Phys. **A556**, 653 (1993).

[17] S. A. Page *et al.*, Phys. Rev. **C35**, 1119 (1987); M. Bini *et al.*, Phys. Rev. Lett. **55**, 795 (1985).

[18] C. S. Wood *et al.*, Science **275**, 1759 (1997).

[19] V. V. Flambaum and D. W. Murray, Phys. Rev. **C56**, 1641 (1997).

[20] W. S. Wilburn and J. D. Bowman, Phys. Rev. **C57**, 3425 (1998).

[21] P. A. Vetter *et al.*, Phys. Rev. Lett. **74**, 2658 (1995).

[22] P. D. Eversheim *et al.*, Phys. Lett. **B256**, 11 (1991).

[23] S. Kistryn *et al.*, Phys. Rev. Lett. **58**, 1616 (1987).

[24] S. A. Page, in "7th Intl. Conf. on Polarization Phenomena in Nuclear Physics", eds. A. Bourdard and Y. Terrien (Colloque de Physique 51, 1990) C6-253; W. T. H. van Oers, in "Future Directions in Particle and Nuclear Physics at Multi-GeV Hadron Beam Facilities", ed. D. F. Geesaman (BNL Report BNL-52389, 1993) p.161.

[25] V. Yuan *et al.*, Phys. Rev. Lett. **57**, 1680 (1986).

[26] N. Lockyer *et al.*, Phys. Rev. **D30**, 860 (1984).

[27] W. T. H. van Oers, Invited Paper presented at 16th International Conference on Few-Body Problems in Physics, Taipei, March 6-10, 2000; and private communication.

[28] J. Alberi *et al.*, Can. J. Phys. **66**, 542 (1988).

[29] V. A. Knyaz'kov *et al.*, Nucl. Phys. **A417**, 209 (1984).

[30] E. D. Earle *et al.*, Can J. Phys. **66**, 534 (1988).

[31] J. D. Bowman (Spokesperson) *et al.*, "Measurement of the Parity-Violating Gamma Asymmetry A_γ in the Capture of Polarized Cold Neutrons by Para-Hydrogen, $\vec{n}+p \to d+\gamma$", Proposal for DOE, 17 April 1998; W. M. Snow *et al.*, Nucl. Inst. Meth. **A444**, 729 (2000).

[32] J. D. Bowman and W. M. Snow, private communication.

[33] JLab LOI 00-002, W. T. H. van Ores and B. Wojtsekhowski, spokespersons (1999).

[34] I. B. Khriplovich and R. V. Korkin, nucl-th/0010032.

[35] J. W. Chen and X. Ji, submitted to Phys. Rev. Lett., hep-ph/0011230; and private communication.

[36] B. R. Holstein, private communication.

[37] R. M. Woloshyn, Can. J. Phys. **57**, 809 (1979).

[38] S. P. Li, E. M. Henley, and W-Y. P. Hwang, Ann. Phys. **143**, 372 (1982).

[39] J. W. Chen and X. Ji, in preparation.

[40] F. A. Berends and D. L. Weaver, Nucl. Phys. **B30**, 575 (1971); M. MacCormick *et al.*, Phys. Rev. **C53**, 41 (1996); J. Ahrens *et al.*, Phys. Rev. Lett. **84**, 5950 (2000).

[41] Charles Sinclair, private communication; The Science Driving the 12 GeV Upgrade of CEBAF, Draft v1.0, p.131.

[42] Hari Areti and Valeri Lebedev, CEBAF accelerator group, private communication.

[43] JLab Proposal E-91-017, D. H. Beck, spokesperson (1991).

[44] K. Aniol *et al.*, Phys. Rev. Lett. **82**, 1096 (1999).

[45] David Meekins, private communication.

[46] P. V. Degtyarenko, M. V. Kossov, and H.-P. Wellisch, Eur. Phys. J. **A8**, 217 (2000).

[47] JLab Proposal E-89-009, R. Chrien, E. Hungerford, and L. Tang, spokespersons (1989).

[48] J. P. Chen and D. Margaziotis, private communication.

[49] D. J. J. de Lange *et al.*, Nucl. Instrum. Meth. **A406**, 182 (1998); D. J. J. de Lange *et al.*, Nucl. Instrum. Meth. **A412**, 254 (1998).

[50] V. Nelyubin *et al.*, "Precision Measurements of Electroproduction of π^0 near Threshold: A Test of Effective Field Theories", Proposal to be submitted to PAC 19; and private communication.

[51] John LeRose, private communication.

[52] Stan Majewski and Paul Souder, private communication.

[53] F. Sauli, Principles of Operation of Multiwire Proportional and Drift Chambers, CERN 77-09 (1977).

[54] National Institute of Standards and Technology, Physical Reference Data, http://physics.nist.gov/PhysRefData.

[55] J. W. Chen and T. D. Cohen, nucl-th/0009031.

[56] E. Bartoš, V. Bytev, and E. Kuraev, hep-ph/0011037.

[57] J. W. Motz *et al.*, Rev. Mod. Phys. **41**, 581 (1969).

[58] JLab Proposal E-99-115, K. Kumar and D. Lhuillier, spokespersons (1999).

[59] JLab Proposal E-00-003, R. Michaels, P. Souder, and G. Urciuoli, spokespersons (2000).

[60] B. K. Kerimov and M. Y. Safin, Sov. J. Nucl. Phys. **42**, 433 (1985).

[61] C. Fronsdal and H. Uberall, Nuovo Cimento **8**, 163 (1958); Phys. Rev. **111**, 580 (1958).

[62] H. Uberall, Phys. Rev. **107**, 223 (1957).

[63] P. Degtyarenko and R. May, Radiation Control Group, private communication.

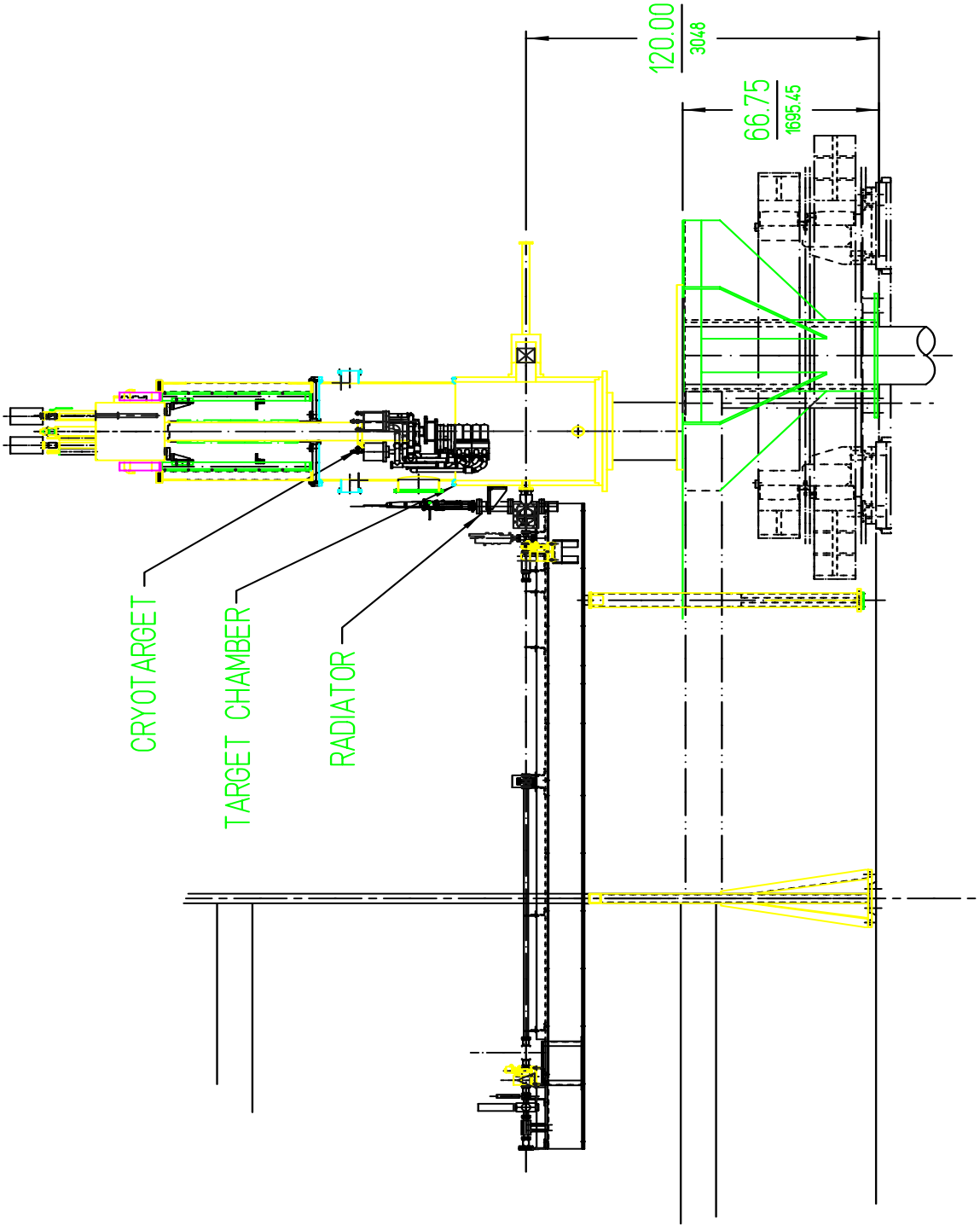

Figure 28: Hall A setup just before installing BigBite magnet.

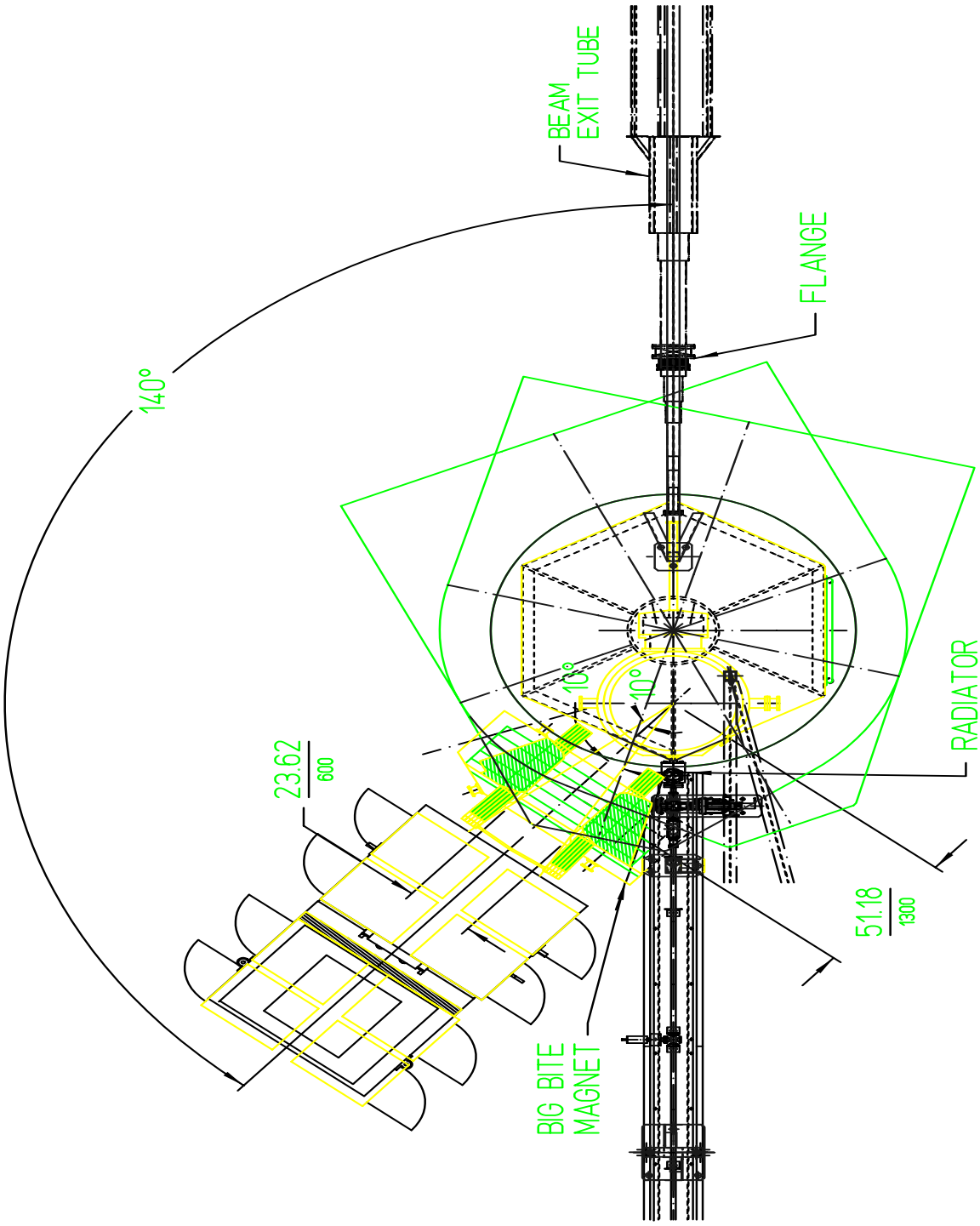

Figure 29: Hall A setup during this experiment. The BigBite magnet will be at 140° and at 1.3 m from the target. The radiator will be moved to be 2 m upstream the target. A sweeping magnet will be installed between the radiator and the target (not shown).

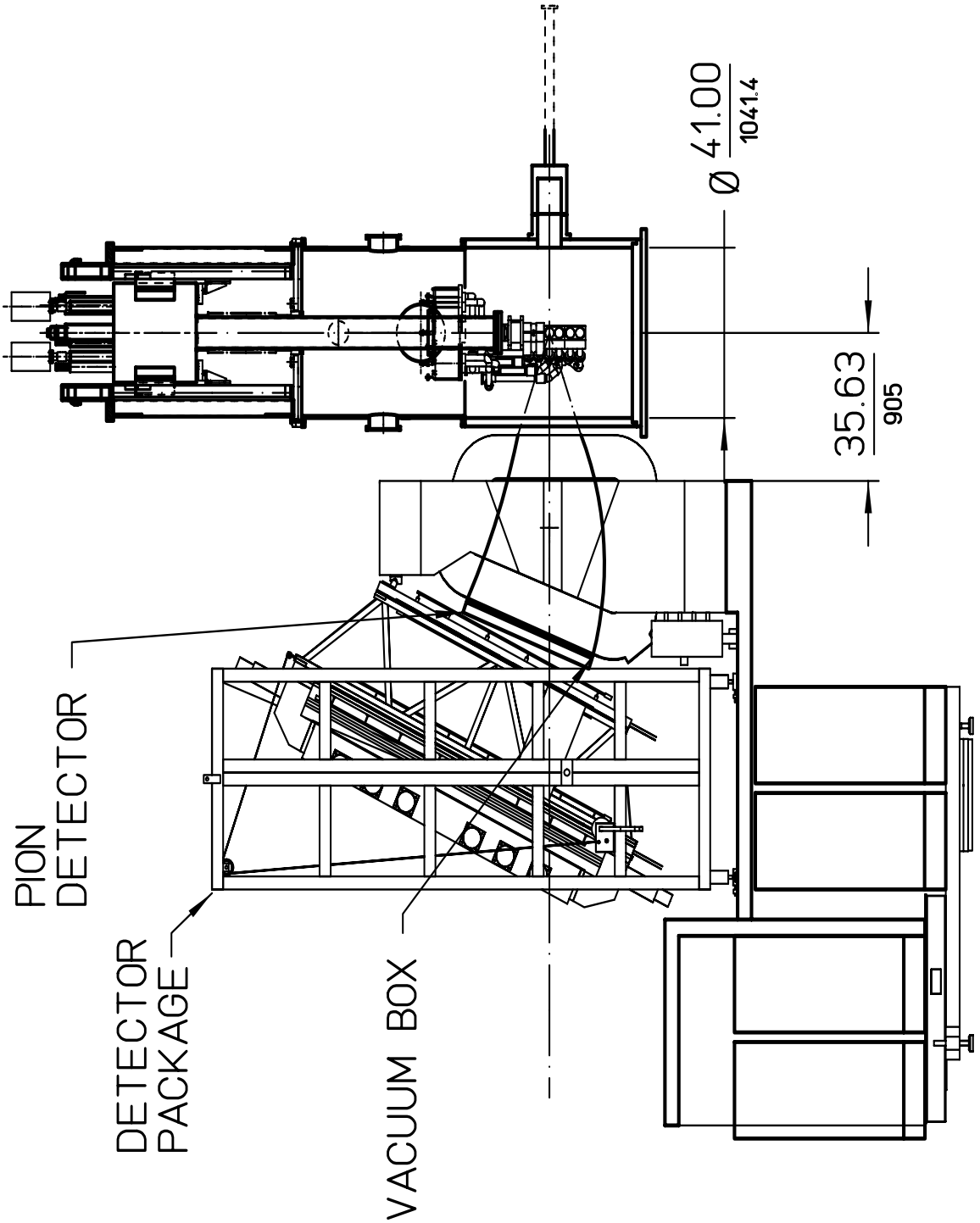

Figure 30: BigBite magnet as used in this experiment. The pion detector will be placed in front of the detector package. Vacuum box will connect the scattering chamber to the pion detector.